36(1/2)

LIBRARY

JAN 2 3 1987

National Marine Fisheries Service
2570 Dole Street
Honolulu, Hawaii

気象庁欧文海洋報告

第36巻 第1-2号

THE OCEANOGRAPHICAL MAGAZINE

Vol. 36 Nos. 1-2

CONTENTS

ENDO, H. and K. SHIGEHARA: Thermodynamic properties of sea water under pressure 1

ISOZAKI, I. and A. SHIBATA: A method of estimating atomospheric water vapor and sea surface wind speed by the microwave radiometer of Marine Observation Satellite—1 17

TAKEUCHI, M.: Sea wave condition of typhoon 8506 and its prognostics in coastal area by the operational coastal wave prediction model of JMA 25

TAKATANI, S., T. SAGI and M. IMAI: Distributions of floating tars and petroleum hydrocarbons at the surface in the western North Pacific 33

KANO, Y.: Preliminary study on sinking particles in the adjacent seas of Tokyo 43

NOTE

SAIKI, M. and K. NAGASAKA: Long-term variation of sea surface temperature in the North Pacific Ocean 51

SAGI, T.: Cadmium and mercury in the seas around Japan 57

Published by the Japan Meteorological Agency

March, 1986

投稿規定

1　資　格

原則として，気象庁職員に限る。ただし，気象庁職員との連名の場合は，この限りでない。

2　論文及び報文（以下「論文等」という）の内容

未発表の原稿で，海洋（物理・化学・生物・地質など）及び海上気象（波浪・海氷・海気相互関係など）に関する論文並びに気象庁における海洋・海上気象業務の活動，そのために開発された測器及び方法に関する報文など。

3　書き方

(1) 用語は，欧文（原則として英文）とする。

(2) 論文等には，英文（300語以内）及び和文（800字以内）の要約を付ける。要約は，方法・測器・実験・観測の結果・仮定・理論などの中味が読みとれるように留意し，なるべく指定の長さで簡潔に書く。

(3) 論文等の始めには，題名・著者名及所属機関名を明記する。和文の要約にも同様のことを明記する。

(4) 原稿は，厚手の用紙にダブルスペースでタイプする。

(5) 図は，白紙又は青方眼紙に墨入れし，図及び図中の文字の大きさは，印刷の際の縮小率を考えて作成する。特に重要な図は，投稿者が大きさを指定する。（印刷の都合上，希望どおりにならないこともある）

(6) 図（写真を含む）及び表には，必ず説明を付ける。図の説明文は，別紙にタイプする。折り込みの図及び表は，なるべく避ける。図及び表のそう入箇所を本文の欄外に記入する。

(7) 数式は，2 行取りに書き，数式の文字及び記号をはっきりと説明する。

(8) 論文等の中に文献を引用する場合は，「ALLEN (1927)」又は「(ALLEN, 1927)」のように書く。

(9) 引用文献は，最後にまとめて付け，著者名のアルファベット順に並べる。書き方は次のようにする。

ALLEN, W.E. (1927): Surface catches of marine diatoms and dinoflagellates made by U.S.A. Pioneer in Alaskan waters in 1923. *Bull. Scripps Inst. Occanogr., Tech. Ser.* **1**(4), 39–48.

BUDYKO, M. I. (1956): *The heat balance of the earth's surface.* Hydrometeorogical Publishing House, Leningrad, pp. 254.

VERONINS, G. and H. STOMMEL (1956): The action of a variable wind stress on a stratified ocean. *J. Mar. Res.*, **15**(1), 43–75.

4　提出方法

投稿票を付け，本稿のほかにコピー（図及び表を含む）2 部を添える。

5　送付先

気象庁海洋気象部海洋課

6　その他

論文等 1 編につき別刷り50部を著者に無料で送付する。

Oceanographical Magazine

編集委員長　Editor

斎　藤　　実，M. SAITO

編集委員　Editorial Board

遠　藤　昌　宏，M. ENDO**
羽　鳥　光　彦，M. HATORI*
川原田　　裕，Y. KAWARADA***
長　坂　昂　一，K. NAGASAKA*
西　山　勝　暢，K. NISHIYAMA*
驚　　猛，T. SAGI*
佐　野　　昭，A. SANO*
杉　村　行　勇，Y. SUGIMURA**
宇　治　　豪，T. UJI**

* 気　象　庁　JAPAN METEOROLOGICAL AGENCY

** 気象研究所　METEOROLOGICAL RESEARCH INSTITUTE

*** 気象大学校　METEOROLOGICAL COLLEGE

The Oceanographical Magazine
Vol. 36, Nos. 1–2, pp. 1 to 15, March 1986

Thermodynamic properties of seawater under pressure

Harumi ENDO
Department of Applied Physics, National Defense Academy
and
Koji SHIGEHARA
Japan Meteororological Agency

(Received December 6, 1985; Accepted January 10, 1986)

Abstract: According to the previous outlined procedure, we splitted the equilibrium thermodynamic quantity (z_0^s) of seawater under pressure into the relaxation (z_r^s) and the instantaneous (z_∞^s) quantity. It is found that the pressure dependence of z_0^s may be expressible in terms of the dehydration of ions. The anomaly of water and seawater is expressible in terms of z_r^s and z_∞^s. On the basis of discussion for z_r^s and z_∞^s, it is found that the dependence of z_0^s on T, P and s is due to the change of water structure. It is obvious that the significant contribution to the change of water structure is attributable to NaCl which is involved in seawater as the most major component. The relaxation mechanism in NaCl-aqueous solution consists of only the ionic hydration where the excess sound absorption is smaller than that of water.

1. Introduction

It has been recognized for us that our knowledge of the physical and chemical properties of seawater is not enough, because it is very difficult to find the dynamical properties of seawater. We usually confine our attention to the seawater system in equilibrium. The reason why the dynamical quantity of seawater can not be found is the lack of the appropriate water and seawater model and also the experiment to find the relaxation processes at very high frequencies. Although the measurements of sound absorption of seawater (FISHER and SIMMONS, 1977; FRANCOIS and GARRISON, 1982; MELLEN *et al.*, 1983) are one of the most useful means to find the dynamical processes of seawater, the dynamical processes so far found are attributable to the electrolytes of $MgSO_4$, H_3BO_3, $MgB(OH)_4^+$, $MgHCO_3^+$, $MgCO_3$ *etc.* and the study of relaxational processes for these salts is limited to very low frequency ranges to serves as SONA. At very high frequencies it is easily expected that another relaxation mechanism, *i.e.*, an ionic hydration, takes place, because the hydrated water molecule moves very quickly. From the measurements of sound absorption and Brillouin scattering for ionic hydration, it is very difficult to find the relaxation process, because of the relaxation frequency with the estimated order of *ca.* 10 GHz at room temperature (KASPER and TAMM, 1980). Also liquid water shows more one order smaller relaxation frequency (ENDO, 1982) than that of the ionic hydration. Therefore great difficulty may be experienced in determining the relaxation quantity of liquid water from the experiments.

In the preceding paper (ENDO and SHIGEHARA, 1983), we proposed a simple model to

split the equilibrium thermodynamic quantity of seawater at atmospheric pressure into the relaxation and instantaneous one. That is to say, assuming the additivity law between the instantaneous quantities of electrolytes in seawater which is an aqueous solution of mixed electrolytes, the relaxation and the instantaneous quantity are determined from our water model (ENDO, 1982) and the electrolyte solution model (ENDO and NOMOTO, 1981) of hydrated water molecules around an ion.

The purpose of the present paper is to demonstrate the usefulness of our seawater model under pressure in estimating the thermodynamic quantities of relaxation and instantaneous. The anomaly of seawater is explained in terms of the relaxation and instantaneous quantities obtained from our calculations.

2. Models for liquid water and electrolyte aqueous solutions, and thermodynamic quantities

ENDO (1982) have shown that the mechanism of sound absorption in liquid water is to be found a double relaxation mechanism due to a rotation and a jump diffusion of water molecules on quasicristalline lattices. Thermodynamic quantities estimated from statistical mechanics are previously obtained. The equilibrium isobar expansibility α_0 is shown in terms of instantaneous α_∞ and relaxation α_r as follows:

$$\alpha_0=\alpha_\infty+\alpha_r \tag{1}$$

and

$$\alpha_r=\frac{C}{VT^2}+\frac{D}{VT^3} \tag{2}$$

where C and D are constant, and V and T are the volume and the absolute temperature, respectively. The relaxation adiabatic compressibility $\beta_{S,r}$ of liquid water is given by

$$\beta_{S,r}=-\frac{4E\alpha_\infty}{TC_{P,0}} \tag{3}$$

and

$$E=C+\frac{D}{T}$$

where $C_{P,0}$ is the equilibrium heat capacity at constant pressure. On the other hand the relaxation isothermal compressibility $\beta_{T,r}$ is given by

$$\beta_{T,r}=-\frac{E(2\alpha_\infty-\alpha_0)}{TC_{P,0}} \tag{4}$$

The relaxation heat capacity at constant pressure $C_{P,r}$ and at constant volume $C_{V,r}$ are

$$C_{P,r}=\frac{E}{T^3V\beta_{T,r}} \tag{5}$$

and

$$C_{V,r}=C_{P,r}+TV\left(\frac{\alpha_\infty{}^2}{\beta_{T,\infty}}-\frac{\alpha_0{}^2}{\beta_{T,0}}\right), \tag{6}$$

respectively. In Eq. (1) the quantities α_∞, C and D are obtainable from the curve fitting of the equilibrium isobar expansibility α_0 of liquid water. This leads to the determination of relaxation quantity z_r such as $\beta_{S,r}$, $\beta_{T,r}$, $C_{P,r}$ and $C_{V,r}$ from Eqs. (3–6). If the quantity z_r is obtainable, the instantaneous quantity z_∞ is computed by the thermodynamic relation-

ship;

$$z_\infty = z_0 - z_r \tag{7}$$

where z_0 is the equilibrium quantity.

It has been known that the structure of liquid water does not seriously change over the entire oceanographic range of pressure to *ca.* 1000 bars (EISENBERG and KAUZMANN, 1969). Thus we can apply our water model (ENDO, 1982) to liquid water under the oceanographic pressure. The results (ENDO *et al.*, 1982) for α_∞, C and D in isobar expansibility under pressure are as follows:

$$\alpha = 1.182206\times10^{-3} + 5.311604\times10^{-8}P - 9.738819\times10^{-11}P^2 - 3.085152\times10^{-13}P^3 + 9.94102\times10^{-17}P^4 - 2.36236\times19^{-20}P^5 + 3.07279\times10^{-24}P^6 [\mathrm{deg}^{-1}]$$

$$C = 8.23287433 - 1.743975\times10^{-1}P + 9.227297\times10^{-5}P^2 + 6.692108\times10^{-5}P^3 - 2.644043\times10^{-11}P^4 + 6.810815\times10^{-15}P^5 - 9.46338\times10^{-19}P^6 [\mathrm{cm^3 deg\ g^{-1}}]$$

$$d = \frac{1 - 2.301391\times10^{-2}P + 1.662749\times10^{-5}P^2 - 1.820101\times10^{-19}P^3}{-3.020633\times10^{-13} + 6.4894053\times10^{-5}P - 5.3738632\times10^{-18}P^2} [\mathrm{deg}]$$

where D equals Cd. Thus we can obtain the relaxation (z_r) and the instantaneous (z_∞) quantities for liquid water under pressure by the use of Eqs. (3–7).

As there are some origins of relaxation processes such as H_3BO_3, ion-pairs (i.p.), $MgSO_4$, ionic hydrations (i.h.), and H_2O in seawater, the relaxation quantity of seawater z_r^s generally consists of these relaxation processes. Thus we have a relation:

$$z_r^s = z_r^{H_3BO_3} + z_r^{i.p} + z_r^{MgSO_4} + z_r^{i.h} + z_r^{H_2O} \tag{8}$$

where the superscripts of z_r correspond to their individual processes. The instantaneous quantity z_∞^s of seawater is given by

$$z_\infty^s = z_0^s - z_r^s \tag{9}$$

where z_0^s is the equilibrium quantity of seawater. No direct measurements of z_r^s for relaxation processes are available for seawater because of the lack of the relaxation curve of seawater over the entire range of frequency. Although the calculation of z_r^s in seawater is technically difficult, it is possible to calculate the z_r^s with some assumptions.

Let us suppose when an electrolyte is dissolved into liquid water. The movement of rotation and translation of water molecules arranged around an ion may be prevented by the electrostriction of the ion because of the large dipole moment of water molecule. This interaction between the ion and the water molecules is known as the ionic hydration. The number of the hydrated water molecule is the hydration number of ion. This hydration leads to the decreases of z_r^w and z_∞^w, where z_r^w and z_∞^w are relaxation and instantaneous quantity of free water, respectively. While the addition of salts results in increasing the instantaneous quantity of salts z_∞^e. Thus we have the expression for the z_∞^s of seawater according to the additivity law of z.

$$z_\infty^s = \frac{s}{1000} z_\infty^e + \frac{1000 - s}{1000} z_\infty^w (1 - x_h) \tag{10}$$

where s is the salinity, x_h the fraction of hydrated water molecules and $(1 - x_h)$ the fraction

of the remaining free water. Here the value of x_h is determined from the hydration number obtained by compressibility (PASSYNSKII, 1938). Equation (10) is based on the following assumptions.

1) The instantaneous quantity z_∞^s of seawater consists of that of ion z_∞^{ion} and of the remaining free water z_∞^w.
2) The z_∞^{ion} equals the instantaneous quantity z_∞^e of salts in seawater.

In the calculation of z_∞^s we assume that the quantity z_∞^e for pressure is a constant because of the narrow range of pressure under the investigations and the small pressure coefficient of z_∞^s.

The instantaneous quantity of adiabatic compressibility $\beta_{S,\infty}^s$ and specific heat of constant volume $C_{V,\infty}^s$ in seawater is obtained from the thermodynamic relationships because of the lack of $\beta_{S,\infty}^e$ and $C_{V,\infty}^e$, respectively.

$$\beta_{S,\infty}^s = \beta_{T,\infty}^s - \frac{T(\alpha_\infty^s)^2}{\rho^s C_{P,0}^s}$$

and (11)

$$C_{V,\infty}^s = C_{P,\infty}^s - \frac{T(\alpha_\infty^s)^2}{\rho^s \beta_{T,\infty}^s}$$

where ρ^s is the density of seawater. On the other hand the relaxation quantity z_r^s of seawater is obtained by use of Eq. (9).

3. Results and discussion

Calculation: Since all of the data set used here is the same as those of our previous work (ENDO and SHIGEHARA, 1983), we abbreviate to show the references for data. The result of our calculation is shown in Table 1.

Thermodynamic parameters shown in Table 1 are in the range of 0°C to 35°C for temperature, of atmospheric pressure to 1000 bars for pressure, and of 0. 25‰ to 40‰ for salinity. The values of r- and ∞-quantity are substantially of the same order of magnitude as those of pure water, decrease with increasing salinity, temperature and pressure.

When the ionic hydration occurs in liquid water, the remaining free water decreases. Thus the ionic hydration leads to the decreases of r- and ∞-quantity of liquid water. Although the quantity z_0^s, in this way, decreases with increasing concentration, there is also another reason why the value of z_∞^e is occasionally smaller than that of z_∞^w.

The relaxation mechanisms of various types in seawater appear with the occurrence of hydrated water molecules, *e.g.*, the consecutive dissociation processes of $MgSO_4$, ion-pairs, the hydrolysis reaction of H_3BO_3, and the ionic hydrations. These species show the acoustic relaxation processes at each specific frequency. These mechanisms are explained in terms of volume relaxation processes (STUEHR and YEAGER, 1965).

The r-value which we obtained is shown in terms of the summation of all the individual relaxation process. The r-quantity of seawater decreases with increasing temperature, pressure and concentration because of the dehydration of an ion, *e.g.*, this relationship is illustrated by the result in the figure of hydration number. On the other hand the de-

Table 1. The quantities z_0, z_T and z_∞ of liquid water and seawater under pressure. The units of α ($\times 10^{-6}$/deg.); C_v, C_p ($\times 10^{-3}$ J/g deg.); and β_T, β_S ($\times 10^{-8}$/bar) are omitted.

	α_∞	α_T	α_0	α_∞	α_T	α_0	α_∞	α_T	α_0	α_∞	α_T	α_0	α_∞	α_T	α_0
T (°C)							S = 0								
0	1160	-1228	-68	1171	-1167	3	1173	-1106	66	1167	-1045	121	1134	-924	209
5	1160	-1144	15	1171	-1097	73	1173	-1048	124	1167	-997	169	1134	-891	242
10	1160	-1072	87	1171	-1037	133	1173	-998	175	1167	-955	212	1134	-861	272
15	1160	-1009	150	1171	-983	187	1173	-953	220	1167	-917	250	1134	-834	299
20	1160	-953	206	1171	-936	235	1173	-912	261	1167	-882	258	1134	-809	325
25	1160	-903	257	1171	-892	278	1173	-874	299	1167	-849	317	1134	-785	349
30	1160	-857	303	1171	-852	318	1173	-839	333	1167	-819	347	1134	-762	272
35	1160	-814	345	1171	-814	356	1173	-806	366	1167	-790	376	1134	-740	394
							S = 25 ‰								
-2			-11			51			107			156			233
0	1065	-1045	19	1079	-1001	77	1084	-955	128	1082	-908	174	1057	-811	245
5	1070	-982	88	1084	-949	134	1089	-913	176	1086	-873	213	1061	-788	272
10	1075	-928	146	1088	-904	183	1093	-876	217	1090	-843	247	1064	-766	297
15	1079	-881	197	1091	-864	227	1096	-842	253	1093	-815	278	1066	-746	319
20	1082	-838	243	1094	-828	266	1099	-811	287	1095	-788	307	1067	-726	340
25	1084	-799	285	1097	-793	303	1101	-781	319	1097	-762	334	1068	-707	361
30	1087	-762	324	1099	-761	337	1103	-753	349	1098	-738	360	1069	-688	381
35	1088	-727	361	1101	-731	369	1104	-726	377	1100	-714	385	1070	-670	400
							S = 30 ‰								
-2			-6			66			120			167			240
0	1047	-1012	35	1061	-970	91	1067	-927	140	1066	-882	183	1043	-790	252
5	1053	-952	101	1067	-921	145	1073	-887	185	1071	-850	220	1047	-769	278
10	1059	-901	157	1072	-880	192	1078	-853	224	1075	-822	253	1050	-749	301
15	1063	-857	206	1076	-842	234	1081	-822	259	1079	-795	283	1053	-729	323
20	1067	-816	250	1080	-807	272	1084	-792	292	1081	-770	311	1054	-711	343
25	1070	-779	291	1083	-775	307	1087	-764	323	1083	-746	337	1056	-692	363
30	1072	-743	329	1085	-744	341	1089	-736	352	1085	-722	363	1057	-673	383
35	1075	-710	364	1087	-714	372	1091	-710	380	1087	-699	388	1058	-655	402
							S = 34 ‰								
-2			19			78			129			175			246
0	1033	-985	48	1048	-946	101	1054	-905	149	1053	-862	191	1032	-774	258
5	1040	-928	111	1054	-900	154	1060	-868	192	1059	-832	226	1036	-753	282
10	1046	-880	165	1060	-860	199	1065	-835	230	1064	-805	258	1040	-735	305
15	1051	-838	212	1064	-825	239	1070	-805	264	1067	-780	287	1042	-716	326
20	1055	-799	255	1068	-791	276	1073	-777	296	1070	-756	314	1044	-698	346
25	1058	-763	295	1071	-760	311	1076	-750	326	1073	-732	340	1046	-680	365
30	1061	-729	332	1074	-730	344	1078	-723	355	1075	-709	365	1047	-662	385
35	1064	-696	367	1076	-700	375	1080	-697	383	1077	-686	390	1048	-644	404
							S = 35 ‰								
-2			23			80			132			177			248
0	1030	-978	51	1044	-940	104	1051	-899	151	1050	-857	193	1029	-770	259
5	1037	-923	114	1051	-894	156	1057	-863	194	1056	-828	228	1034	-750	284
10	1043	-875	167	1057	-855	201	1062	-831	231	1061	-801	259	1037	-731	306
15	1048	-833	214	1061	-820	241	1067	-801	265	1065	-777	288	1040	-713	326
20	1052	-795	257	1065	-787	277	1070	-773	297	1068	-753	315	1042	-695	346
25	1056	-759	296	1069	-756	312	1073	-746	327	1070	-729	341	1043	-677	366
30	1058	-725	333	1071	-726	344	1076	-720	355	1072	-706	366	1045	-659	385
35	1061	-692	368	1073	-697	376	1078	-694	383	1074	-683	390	1046	-641	404

P (bar)	1			200			400			600			1000		
	$C_{V,\infty}$	$C_{V,r}$	$C_{V,0}$	$C_{V,\infty}$	$C_{V,r}$	$C_{V,0}$	$C_{V,\infty}$	$C_{V,r}$	$C_{V,0}$	$C_{V,\infty}$	$C_{V,r}$	$C_{V,0}$	$C_{V,\infty}$	$C_{V,r}$	$C_{V,0}$
T (°C)							S = 0								
0	894	3319	4214	834	3286	4122	803	3242	4045	796	3182	3979	851	3114	3866
5	935	3266	4202	865	3252	4117	822	3223	4045	808	3176	3983	855	3021	3877
10	973	3213	4187	892	3217	4109	839	3202	4041	817	3166	3983	855	3026	3882
15	1011	3159	4171	919	3179	4098	855	3178	4134	825	3135	3978	854	3028	3883
20	1049	3104	4154	946	3138	4084	873	3151	4024	834	3136	3971	854	3025	3880
25	1089	3046	4135	975	3095	4070	892	3120	4012	845	3115	3961	856	3018	3874
30	1128	2986	4115	1005	3048	4053	914	3084	3998	859	3089	3949	859	3007	3867
35	1171	2923	4094	1037	2997	4034	937	3045	3982	875	3059	3935	865	2992	3857
							S = 25 ‰								
0	861	3187	4048	810	3161	3972	782	3122	3905	778	3068	3847	833	2917	3750
5	902	3135	4038	837	3131	3969	804	3104	3908	793	3062	3855	840	2926	3767
10	941	3086	4028	870	3093	3964	823	3084	3908	805	3053	3858	843	2931	3774
15	980	3037	4017	898	3059	3957	842	3062	3904	815	3041	3856	845	2930	3776
20	1019	2986	4005	926	3022	3948	860	3036	3897	826	3025	3851	846	2926	3773
25	1057	2933	3991	955	2981	3937	880	3007	3888	838	3005	3844	849	2917	3767
30	1097	2877	3975	985	2938	3923	902	2973	3876	853	2980	3833	854	2905	3759
35	1138	2818	3957	1013	2894	3907	925	2936	3862	869	2951	3821	860	2888	3748
							S = 30 ‰								
0	854	3161	4016	806	3136	3942	779	3099	3878	775	3046	3822	830	2899	3729
5	896	3111	4007	836	3104	3940	800	3081	3882	790	3040	3831	837	2907	3745
10	935	3062	3998	866	3070	3936	820	3062	3882	802	3031	3834	841	2912	3753
15	974	3014	3988	892	3038	3930	839	3039	3879	813	3019	3833	843	2911	3754
20	1012	2964	3977	922	2999	3922	858	3014	3872	824	3003	3828	845	2906	3751
25	1051	2912	3964	951	2959	3911	878	2985	3863	837	2983	3820	848	2896	3745
30	1091	2857	3948	981	2916	3897	900	2951	3851	851	2958	3809	853	2883	3736
35	1132	2798	3930	1013	2868	3881	923	2913	3837	868	2928	3796	859	2865	3724
							S = 34 ‰								
0	849	3141	3991	802	3117	3919	775	3081	3857	772	3030	3803	827	2885	3712
5	891	3091	3983	833	3085	3918	798	3063	3861	788	3023	3812	835	2893	3729
10	930	3044	3974	862	3052	3914	817	3044	3862	800	3014	3815	839	2897	3736
15	969	2996	3965	890	3018	3909	837	3022	3859	811	3002	3814	841	2895	3737
20	1007	2947	3955	919	2982	3901	856	2997	3853	823	2986	3809	843	2890	3734
25	1046	2895	3942	948	2942	3890	876	2967	3843	835	2965	3801	847	2880	3727
30	1086	2841	3927	977	2899	3877	898	2933	3831	850	2939	3790	852	2865	3717
35	1127	2782	3909	1009	2851	3861	921	2895	3816	867	2909	3776	858	2846	3704
							S = 35 ‰								
0	848	3136	3984	801	3112	3914	775	3076	3852	772	3025	3798	827	2881	3708
5	890	3086	3976	832	3080	3912	797	3059	3856	787	3019	3807	835	2889	3724
10	929	3039	3968	861	3047	3909	817	3040	3857	800	3010	3810	838	2893	3734
15	968	2991	3959	889	3014	3904	836	3017	3854	811	2998	3809	841	2891	3733
20	1006	2943	3949	918	2978	3896	855	2992	3848	823	2981	3804	843	2886	3729
25	1045	2891	3937	947	2938	3885	875	2963	3839	835	2960	3796	846	2875	3722
30	1084	2837	3922	977	2895	3872	897	2929	3826	850	2935	3785	851	2860	3712
35	1125	2778	3904	1008	2846	3855	920	2890	3811	866	2904	3771	858	2841	3699

P (bar)	1			200			400			600			1000		
	$C_{p,\infty}$	$C_{p,r}$	$C_{p,0}$	$C_{p,\infty}$	$C_{p,r}$	$C_{p,0}$	$C_{p,\infty}$	$C_{p,r}$	$C_{p,0}$	$C_{p,\infty}$	$C_{p,r}$	$C_{p,0}$	$C_{p,\infty}$	$C_{p,r}$	$C_{p,0}$
T (°C)							S = 0								
0	2048	2168	4216	2064	2058	4122	2083	1964	4048	2103	1884	3988	2146	1749	3895
5	2115	2086	4202	2127	1993	4121	2141	1913	4055	2158	1844	4002	2194	1724	3918
10	2178	2013	4192	2185	1935	4121	2194	1867	4061	2207	1806	4013	2236	1699	3936
15	2238	1947	4185	2239	1881	4121	2244	1822	4067	2252	1770	4022	2276	1674	3950
20	2295	1886	4181	2291	1831	4122	2291	1781	4072	2295	1734	4030	2312	1650	3963
25	2350	1829	4179	2340	1783	4124	2336	1740	4076	2336	1700	4036	2347	1625	3973
30	2402	1775	4177	2388	1738	4126	2378	1701	4080	2375	1667	4042	2381	1600	3982
35	2454	1723	4177	2434	1693	4128	2420	1664	4084	2412	1634	4046	2413	1575	3989
							S = 25 ‰								
-2			4052			3973			3908			3855			3776
0	1897	2150	4048	1918	2057	3975	1941	1974	3915	1966	1900	3866	2017	1775	3793
5	1969	2073	4043	1985	1995	3980	2004	1924	3928	2024	1861	3885	2068	1752	3821
10	2035	2006	4041	2047	1939	3986	2060	1878	3939	2077	1823	3900	2114	1727	3841
15	2098	1944	4042	2104	1887	3992	2113	1835	3949	2125	1786	3912	2155	1700	3855
20	2157	1887	4044	2158	1839	3997	2162	1794	3957	2170	1751	3922	2192	1674	3866
25	2213	1833	4047	2209	1793	4002	2208	1754	3963	2212	1718	3930	2227	1648	3875
30	2267	1781	4049	2257	1749	4006	2252	1716	3969	2251	1684	3936	2261	1621	3883
35	2319	1730	4050	2304	1705	4009	2294	1679	3973	2290	1651	3941	2293	1594	3888
							S = 30 ‰								
-2			4020			3944			3883			3833			3757
0	1869	2147	4017	1891	2056	3947	1915	1975	3890	1940	1903	3844	1993	1781	3774
5	1941	2072	4013	1958	1995	3954	1978	1926	3904	2000	1864	3864	2045	1757	3802
10	2008	2005	4013	2020	1939	3960	2035	1880	3916	2053	1826	3879	2091	1731	3822
15	2071	1944	4016	2076	1888	3965	2088	1837	3926	2101	1789	3891	2132	1704	3836
20	2130	1888	4019	2132	1840	3973	2137	1796	3934	2146	1754	3900	2169	1677	3847
25	2187	1834	4022	2184	1795	3979	2184	1756	3941	2188	1720	3908	2204	1650	3855
30	2241	1783	4025	2232	1750	3983	2228	1718	3946	2228	1686	3914	2238	1623	3862
35	2293	1733	4026	2279	1707	3986	2270	1680	3950	2266	1652	3918	2271	1595	3866
							S = 34 ‰								
-2			3994			3922			3863			3815			3743
0	1847	2145	3992	1869	2056	3925	1894	1977	3871	1920	1906	3826	1975	1784	3760
5	1919	2070	3990	1937	1995	3933	1957	1927	3885	1980	1866	3847	2027	1760	3788
10	1986	2004	3991	2000	1940	3940	2015	1882	3898	2034	1828	3862	2073	1734	3807
15	2050	1944	3995	2058	1889	3848	2069	1839	3908	2082	1791	3874	2114	1707	3821
20	2110	1889	3999	2112	1842	3954	2118	1798	3916	2128	1756	3884	2151	1679	3831
25	2166	1835	4002	2164	1796	3960	2165	1758	3923	2170	1721	3891	2187	1651	3839
30	2220	1784	4005	2212	1752	3964	2209	1719	3928	2209	1687	3897	2221	1623	3844
35	2272	1734	4007	2252	1708	3967	2251	1681	3932	2248	1652	3900	2253	1595	3848
							S = 35 ‰								
-2			3988			3917			3858			3811			3740
0	1842	2144	3986	1864	2056	3920	1889	1977	3866	1915	1906	3822	1970	1785	3756
5	1914	2070	3984	1932	1995	3928	1952	1928	3881	1975	1867	3842	2022	1761	3784
10	1981	2004	3986	1995	1940	3935	2010	1882	3893	2029	1828	3858	2068	1735	3804
15	2045	1944	3989	2053	1890	3943	2064	1839	3903	2078	1792	3870	2111	1707	3817
20	2104	1889	3994	2107	1842	3950	2113	1798	3912	2123	1756	3879	2147	1680	3827
25	2161	1836	3997	2159	1796	3955	2160	1758	3919	2165	1721	3887	2182	1652	3835
30	2215	1785	4001	2207	1752	3960	2204	1719	3924	2205	1687	3892	2216	1624	3840
35	2267	1735	4003	2254	1708	3963	2246	1681	3927	2243	1652	3896	2248	1595	3844

P (bar)	1			200			400			600			1000		
	$\beta_{T,\infty}$	$\beta_{T,r}$	$\beta_{T,0}$	$\beta_{T,\infty}$	$\beta_{T,r}$	$\beta_{T,0}$	$\beta_{T,\infty}$	$\beta_{T,r}$	$\beta_{T,0}$	$\beta_{T,\infty}$	$\beta_{T,r}$	$\beta_{T,0}$	$\beta_{T,\infty}$	$\beta_{T,r}$	$\beta_{T,0}$
T (°C)						S = 0									
0	3188	1901	5089	3022	1792	4814	2883	1671	4554	2769	1542	4311	2597	1277	3874
5	3172	1745	4917	2995	1665	4661	2850	1569	4419	2732	1461	4193	2561	1228	3789
10	3164	1617	4781	2978	1560	4538	2825	1484	4310	2704	1394	4097	2530	1187	3717
15	3164	1509	4673	2969	1471	4439	2810	1412	4221	2683	1336	4019	2506	1151	3658
20	3174	1415	4589	2969	1393	4362	2803	1348	4151	2671	1285	3956	2489	1119	3608
25	3191	1335	4525	2978	1324	4301	2804	1291	4096	2667	1239	3906	2479	1090	3569
30	3217	1260	4477	2994	1262	4256	2814	1240	4054	2671	1196	3868	2475	1063	3537
35	3251	1193	4444	3019	1205	4224	2831	1192	4023	2682	1157	3839	2477	1037	3514
						S = 25 ‰									
-2			4821			4564			4324			4101			3697
0	2931	1825	4757	2788	1719	4507	2668	1606	4274	2570	1487	4057	2425	1239	3665
5	2931	1688	4619	2766	1618	4384	2649	1516	4166	2547	1415	3962	2400	1194	3594
10	2936	1572	4508	2771	1513	4285	2636	1441	4077	2529	1354	3884	2377	1157	3534
15	2946	1474	4421	2772	1433	4206	2630	1376	4006	2516	1303	3820	2359	1125	3484
20	2964	1388	4353	2779	1363	4143	2629	1319	3949	2510	1257	3768	2346	1096	3443
25	2987	1314	4301	2794	1301	4095	2635	1268	3904	2511	1215	3727	2339	1070	3409
30	3017	1246	4264	2814	1245	4059	2649	1220	3869	2518	1176	3695	2338	1045	3383
35	3054	1185	4240	2832	1201	4034	2669	1175	3845	2532	1139	3671	2342	1022	3364
						S = 30 ‰									
-2			4755			4504			4270			4052			3657
0	2883	1810	4694	2744	1705	4450	2628	1594	4222	2533	1476	4010	2394	1232	3627
5	2885	1676	4561	2734	1597	4332	2611	1506	4118	2512	1407	3919	2370	1188	3559
10	2892	1562	4455	2731	1504	4236	2600	1433	4033	2496	1347	3844	2348	1152	3501
15	2904	1467	4371	2734	1426	4160	2595	1369	3964	2485	1297	3782	2331	1120	3452
20	2924	1382	4306	2743	1357	4101	2596	1313	3910	2480	1252	3732	2319	1092	3412
25	2948	1309	4258	2758	1296	4054	2603	1263	3867	2481	1211	3692	2313	1066	3379
30	2979	1243	4222	2779	1241	4020	2617	1216	3834	2489	1172	3662	2312	1042	3354
35	3016	1182	4199	2807	1189	3996	2637	1172	3810	2503	1135	3639	2316	1019	3335
						S = 34 ‰									
-2			4704			4457			4227			4013			3626
0	2845	1798	4644	2709	1695	4404	2596	1585	4181	2504	1468	3973	2369	1227	3597
5	2849	1666	4515	2702	1588	4290	2581	1498	4080	2485	1400	3885	2347	1183	3530
10	2858	1555	4413	2700	1497	4198	2571	1426	3998	2470	1341	3812	2326	1147	3474
15	2871	1460	4332	2704	1420	4125	2568	1363	3932	2460	1292	3752	2310	1116	3427
20	2892	1377	4270	2714	1352	4067	2570	1308	3879	2456	1247	3704	2298	1088	3387
25	2917	1306	4223	2730	1292	4022	2578	1259	3837	2458	1207	3665	2292	1063	3356
30	2948	1240	4189	2752	1237	3989	2593	1212	3805	2466	1169	3635	2291	1039	3331
35	2986	1180	4167	2780	1186	3966	2613	1169	3782	2480	1133	3613	2296	1016	3313
						S = 35 ‰									
-2			4691			4445			4217			4004			3618
0	2836	1795	4632	2701	1692	4393	2588	1582	4171	2497	1466	3964	2363	1226	3589
5	2840	1663	4504	2693	1586	4280	2574	1496	4071	2478	1398	3876	2341	1182	3523
10	2849	1553	4402	2693	1495	4188	2564	1424	3989	2464	1340	3804	2320	1146	3467
15	2863	1459	4322	2697	1418	4116	2561	1362	3924	2454	1290	3745	2304	1115	3420
20	2884	1376	4261	2707	1351	4059	2564	1307	3871	2450	1246	3697	2293	1088	3381
25	2909	1305	4214	2723	1291	4015	2572	1258	3830	2452	1206	3658	2287	1062	3350
30	2941	1239	4181	2745	1237	3982	2586	1212	3798	2460	1168	3629	2286	1038	3325
35	2978	1180	4158	2773	1185	3959	2607	1168	3776	2474	1132	3607	2291	1016	3307

P (bar)	1			200			400			600			1000		
	$\beta_{S,\infty}$	$\beta_{S,r}$	$\beta_{S,0}$	$\beta_{S,\infty}$	$\beta_{S,r}$	$\beta_{S,0}$	$\beta_{S,\infty}$	$\beta_{S,r}$	$\beta_{S,0}$	$\beta_{S,\infty}$	$\beta_{S,r}$	$\beta_{S,0}$	$\beta_{S,\infty}$	$\beta_{S,r}$	$\beta_{S,0}$
T (°C)							S = 0.								
0	1393	3693	5085	1224	3590	4814	1112	3440	4551	1048	3253	4301	1030	2815	3845
5	1402	3514	4917	1219	3438	4657	1095	3314	4409	1023	3151	4174	998	2750	3749
10	1414	3362	4776	1216	3309	4525	1080	3208	4289	1000	3066	4066	968	2698	3666
15	1430	3227	4658	1218	3197	4415	1072	3116	4188	983	2992	3975	941	2653	3595
20	1452	3108	4559	1226	3096	4323	1069	3034	4103	971	2927	3898	919	2613	3533
25	1479	2999	4477	1240	3005	4246	1072	2959	4031	966	2867	3833	903	2577	3480
30	1512	2898	4410	1261	2921	4182	1081	2891	3972	966	2812	3779	893	2542	3436
35	1551	2804	4355	1287	2843	4129	1097	2826	3923	973	2760	3733	888	2509	3398
							S = 25 ‰								
-2			4820			4562			4316			4084			3662
0	1330	3425	4755	1178	3324	4503	1076	3186	4263	1018	3017	4036	1002	2623	3625
5	1343	3269	4612	1167	3204	4371	1063	3080	4144	997	2932	3930	975	2567	3543
10	1358	3134	4493	1178	3082	4261	1053	2991	4044	980	2860	3840	948	2525	3473
15	1376	3016	4393	1183	2985	4168	1048	2911	3959	965	2799	3765	925	2489	3414
20	1400	2909	4310	1193	2898	4091	1046	2841	3888	956	2744	3700	906	2457	3363
25	1427	2812	4240	1208	2817	4026	1051	2777	3828	952	2693	3645	892	2427	3319
30	1460	2722	4183	1228	2743	3972	1061	2716	3778	954	2645	3599	883	2398	3282
35	1499	2637	4136	1245	2683	3928	1077	2659	3736	961	2599	3561	878	2371	3250
							S = 30 ‰								
-2			4755			4502			4260			4032			3620
0	1317	3375	4693	1169	3275	4444	1069	3139	4208	1012	2973	3986	997	2587	3584
5	1332	3223	4555	1168	3149	4317	1057	3036	4094	992	2891	3884	970	2533	3504
10	1347	3223	4440	1170	3040	4211	1047	2950	3997	976	2822	3798	944	2492	3437
15	1366	2977	4343	1174	2947	4122	1043	2873	3916	961	2763	3725	922	2458	3380
20	1389	2872	4262	1186	2860	4047	1042	2805	3847	953	2710	3663	903	2428	3331
25	1417	2777	4195	1201	2782	3984	1046	2742	3789	949	2660	3610	889	2399	3289
30	1450	2689	4139	1221	2710	3932	1057	2683	3741	951	2613	3565	880	2371	3252
35	1489	2695	1248	1248	2641	3889	1072	2628	3701	958	2569	3528	876	2345	3222
							S = 34 ‰								
-2			4704			4454			4260			3992			3587
0	1308	3335	4643	1162	3236	4398	1069	3139	4208	1008	2939	3947	992	2559	3552
5	1322	3186	4509	1161	3113	4275	1057	3036	4094	988	2859	3848	967	2506	3474
10	1338	3058	4397	1164	3007	4172	1047	2950	3997	972	2791	3764	941	2467	3409
15	1357	2945	4303	1170	2914	4085	1043	2873	3916	968	2734	3693	919	2434	3354
20	1381	2843	4224	1180	2831	4012	1042	2805	3847	950	2683	3633	901	2405	3306
25	1409	2750	4159	1196	2754	3951	1046	2742	3789	947	2634	3581	888	2377	3265
30	1442	2663	4105	1216	2684	3900	1057	2683	3741	949	2589	3538	879	2350	3230
35	1480	2581	4062	1242	2616	3859	1072	2628	3701	956	2545	3502	874	2325	3200
							S = 35 ‰								
-2			4692			4442			4205			3982			3579
0	1305	3325	4631	1160	3226	4387	1062	3093	4155	1006	2930	3937	991	2552	3544
5	1320	3177	4498	1160	3104	4264	1051	2993	4045	987	2851	3839	966	2500	3466
10	1336	3050	4387	1163	2999	4162	1042	2910	3952	971	2784	3756	941	2461	3402
15	1355	2938	4293	1168	2907	4076	1038	2836	3874	958	2727	3686	919	2428	3347
20	1379	2836	4215	1179	2824	4003	1037	2769	3807	949	2676	3626	900	2399	3300
25	1407	2743	4150	1195	2747	3942	1042	2709	3751	946	2628	3575	887	2372	3259
30	1440	2656	4097	1214	2677	3892	1053	2651	3704	948	2582	3531	878	2345	3224
35	1478	2575	4053	1241	2610	3851	1068	2597	3666	956	2539	3495	874	2320	3194

crease of *r*-quantity of seawater is also responsible for the lack of free water with an increase in concentration. Even if there is the slight increment of *r*-quantity for each mechanism, this contribution to the overall *r*-quantity is not so significant to comparison with the decrease of *r*-quantity in pure water by the ionic hydration because of the small amount of salts in seawater. On the other hand with increasing concentration, temperature and pressure, the ∞-quantity of seawater decreases because of the dehydration of ions and also the smalle value of ∞-quantity of salts.

Some of results may be illustrated in details by the use of figures.

Hydration number: The hydration number of ion is an important quantity to elucidate the model of action of hydration around the ion. The value is calculated from the compressibility of seawater. In Fig. 1, the hydration number per 1 g salt is shown as a function of pressure. The hydration number decreases with increasing pressure, of which effect is responsible for the restriction of molecular movements in water molecules. Then

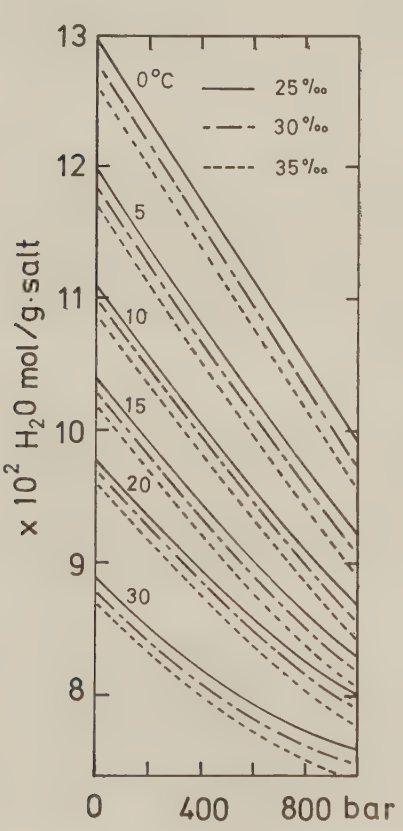

Fig. 1.

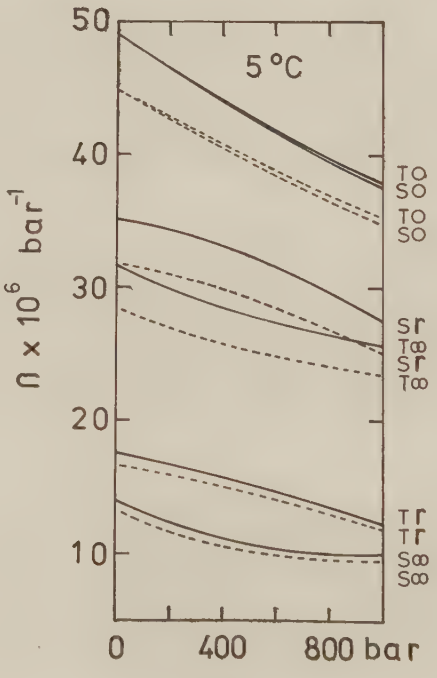

Fig. 2.

Fig. 1. Pressure dependence of hydration number of seawater.
Fig. 2. Pressure dependence of compressibility of liquid water and 35‰-seawater at 5°C.

the decrease of hydration number with increasing pressure is related to the decrease of sound absorption (SCHULKIN and MARSH, 1962). This fact is of important for the sound propagation in ocean. Since the excess sound absorption decreases with increasing pressure, the sound waves at deep sea easily propagate for distance without the exhaust of sound energy.

Compressibility: The compressibility of seawater is also an important quantity in computing the adiabatic temperature changes with pressure $(\partial T/\partial P)_{S,0}$ (ENDO and SHIGEHARA, 1986; ENDO, 1986) in ocean.

Figure 2 shows the dependence of the compressibility on pressure for water and seawater of 35‰ at 5°C. In this figure it is found that the following thermodynamic requirements (ENDO, 1980) is satisfied:

$$\beta_{T,0} > \beta_{S,0} > \beta_{S,r} > \beta_{T,r}$$

and (12)

$$\beta_{T,\infty} > \beta_{S,\infty}$$

To decrease free water by ionic hydration leads to results of $\beta_{T,\infty}{}^{w} > \beta_{T,\infty}{}^{s}$ and $\beta_{S,\infty}{}^{w} > \beta_{S,\infty}{}^{s}$. Since seawater involves NaCl in much larger quantity than the other salts, the excess sound absorption due to hydration of NaCl is less than that of water because NaCl has no relaxation process other than hydration (ENDO and NOMOTO, 1981). Thus we have the relationships of $\beta_{S,r}{}^{w} > \beta_{S,r}{}^{s}$ and $\beta_{T,r}{}^{w} > \beta_{T,r}{}^{s}$. It seem from Fig. 2 that $\Delta\beta_{T,\infty}(s) > \Delta\beta_{T,r}(s)$, where $\Delta\beta_{T,\infty}(s) = \beta_{T,\infty}{}^{w} - \beta_{T,\infty}{}^{s}$ and $\Delta\beta_{T,r}(s) = \beta_{T,r}{}^{w} - \beta_{T,r}{}^{s}$. This fact is explainable from the relation mentioned above.

The relationship between $\beta_{S,r}$ and $\beta_{T,r}$ is given by

$$\beta_{S,r} = \beta_{T,r} + (\Delta\beta_{\infty} - \Delta\beta_{0}) \tag{13}$$

with

$$\left.\begin{aligned} \Delta\beta_{\infty} &= \frac{T\alpha_{\infty}{}^{2}}{\rho C_{P,\infty}} = \beta_{S,\infty}(\gamma_{\infty} - 1) \\ \Delta\beta_{0} &= \frac{T\alpha_{0}{}^{2}}{C_{P,0}} = \beta_{S,0}(\gamma_{0} - 1) \end{aligned}\right\} \tag{14}$$

where γ is the ratio of specific heat. Since $\gamma_0 \cong 1$ for water and seawater, we have

$$\beta_{S,r} \cong \beta_{T,r} + \Delta\beta_{\infty} \tag{15}$$

The result of 35‰-seawater at atmospheric pressure is shown in Fig. 3. It seems that the quantity $T\alpha_0{}^2/\rho C_{P,0}$ is negligible small, thus we have the relations of $\beta_{T,0} \gtrsim \beta_{S,0}$ and $\beta_{S,r} > \beta_{T,r}$. From Eq. (15) the relaxation compressibility is related to the instantaneous adiabatic change of temperature with pressure change $(\partial T/\partial P)_{S,\infty}$ is expressible as follows:

$$\beta_{S,r} \cong \beta_{T,r} + \alpha_{\infty}\left(\frac{\partial T}{\partial P}\right)_{S,\infty} \tag{16}$$

where $(\partial T/\partial P)_{S,\infty}$ equals $T\alpha_{\infty}/\rho C_{P,\infty}$.

In β–T curve the anomaly of water shows the minimum compressibility at *ca.* 64°C for $\beta_{S,0}$ and *ca.* 47°C for $\beta_{T,0}$. This temperature ($T_m(\beta)$) in the minimum compressibility shifts to lower temperatures with increasing concentration and pressure. Since the $T_m(\beta)$ for seawater nearly equals that of pure water, the anomaly of compressibility at such a high temperature is out of the interest for oceanographers.

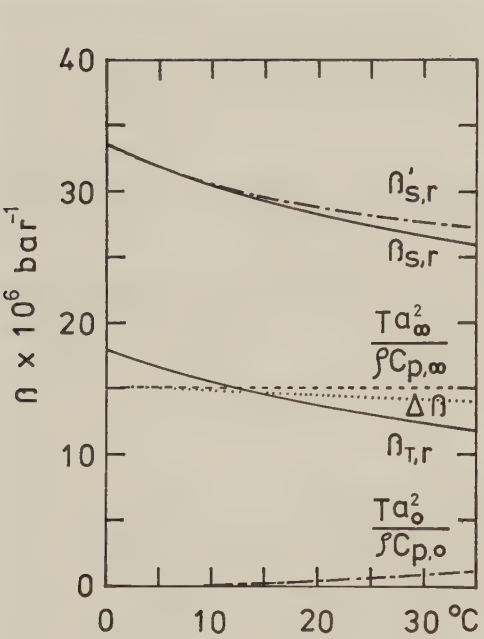

Fig. 3.

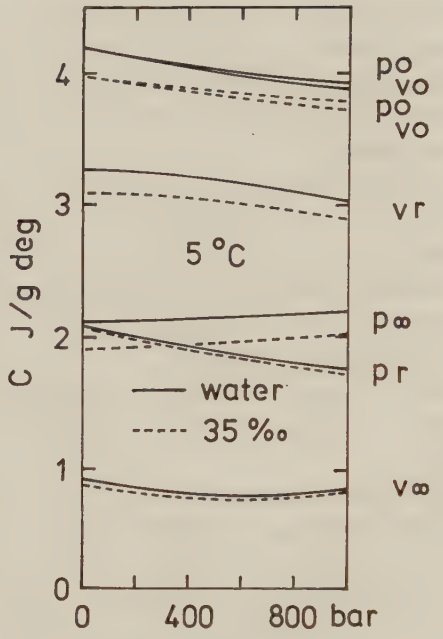

Fig. 4.

Fig. 3. Temperature dependence of compressibility of 35‰-seawater at the atmospheric pressure.

Fig. 4. Pressure dependence of heat capacity of liquid water and 35‰-seawater at 5°C.

Heat capacity: The specific heat of seawater depends on temperature, salinity and pressure. The effect of pressure on the specific heat at constant pressure has been computed for the equation

$$C_P = C_P(0) - T\int_0^P (\partial^2 V/\partial T^2)dP$$

where $C_P(0)$ is the value of C_P at atmospheric pressure.

The pressure dependences of specific heat of liquid water and 35‰-seawater at 5°C are shown in Fig. 4. The quantity $C_{P,r}{}^s$ is responsible for the thermal relaxation processes in seawater. The decrease of $C_{P,r}{}^s$ with increasing concentration is due to the decrease of $C_{P,r}{}^w$ of pure water by the ionic hydration.

The curve of $C_{P,0}-T$ has a small minimum which is denoted by a downward arrow is shown in Fig. 5. The origin of minimum is explainable in terms of $C_{P,\infty}$ and $C_{P,r}$ vs. temperature curves because the temperature dependences of both quantities are opposite for each other. This fact is shown in Fig. 5 in the case of pure water and 35‰-seawater at atmospheric pressure. Table 2 shows the minimum temperature $T_m(C_P)$ in $C_{P,0}$ vs. T curves and the value at $T_m(C_P)$. With increasing concentration $T_m(C_P)$ shifts to lower temperatures. This mechanism results in the destruction of liquid water due to

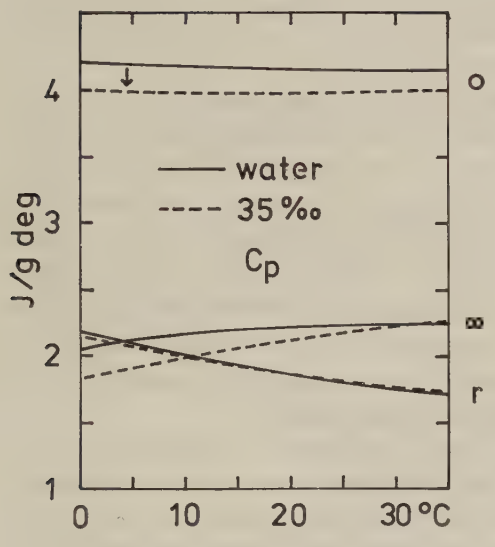

Fig. 5.

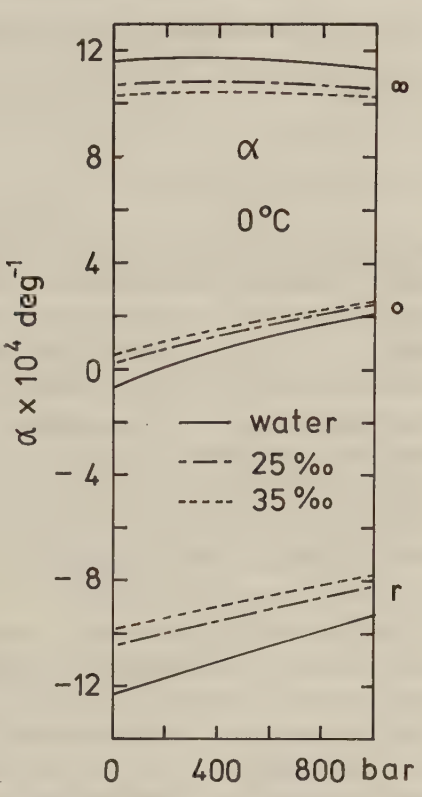

Fig. 6.

Fig. 5. Temperature dependence of heat capacity C_p of liquid water and 35‰-seawater at atmospheric pressure. Arrow shows the minimum temperature.

Fig. 6. Pressure dependence of isobar expansibility of liquid water and 25, 35‰-seawater at 0°C.

Table 2. The values of $T_m(C_P)$ and C_P at T_m for liquid water and seawater.

s	0	25	30	34	35	40
$T_m(C_P)$ (°C)	35	10	7	4	4	2
C_P at T_m (J/g deg.)	4.178	4.042	4.101	3.990	3.985	3.956

the ionic hydration. The dependence of $T_m(C_P)$ on pressure is also given in Table 2.

Isobar expansibility: Pressure dependence of isobar expansibility is shown in Fig. 6. The anomaly in pure liquid water is observable from the figure. This anomaly is responsible for the structure of liquid water where α_r and α_∞ are negative and positive, respectively. The changes of temperature, pressure and salinity affect the structure of liquid water by the breakdown of hydrogen bond, the distortion of hydrogen bond angle and hydration, respectively. Thus the change of T, P and salinity leads to that of α_r and α_∞ from the standard state of liquid water. Since the negative value of α_0 is found only at

Table 3. The temperature at the maximum density $T_m(\rho)$ (°C) of liquid water and seawater

Pressure \ S	0	25
0 bar	3.98	−1.6
100	1.9	
200	−0.4	

low salinities, low temperatures and low pressures, seawater under natural conditions always expands with increasing temperature because of $\alpha_\infty > \alpha_r$. Table 3 shows the upper limit ($T_u(\alpha_0)$) of temperature of anomaly for α_0.

Anomaly: In water and aqueous solutions of electrolyte and nonelectrolyte, we observe anomaly in sound velocity, compressibility, density, isobar expansibility, and heat capacity at constant pressure. These quantities show a minimum, maximum or negative value which shifts with changing conditions. All of the anomaly in water and aquenous solutions are explainable in terms of z_r and z_∞, and its mechanism is responsible for the change of liquid water structure. Although the origin of anomaly is phynominologically classified into the breakdown of hydrogen bond by temperature, the distortion of hydrogen bond, that of bond angle and the rupture of hydrogen bond by pressure, the ionic hydration of electrolyte and the hydrophobic interaction of nonelectrolyte, the anomaly which we observe naturally may be shown by the mixture of their origins.

Liquid water under pressure: When liquid water is compressed, the net effect of pressure is the resultant of the direct contraction (O—O hydrogen bond) and indirect expansion (O—O stretching and O—O—O angle bending) (Whalley, 1975). This leads to the diminish of coupling between the rotational and translational motion of water molecules (DeFries and Jonas, 1977; Jonas, 1982). Strickt speaking we can not applicable our model at atmospheric pressure to the water model under pressure to find the z_r^w and z_∞^w. However it is to be emphasized that our assumption is true only in the pressure range of oceanographic interest because in this range the significant change of structure of liquid water does not occur (Eisenberg and Kauzmann, 1969).

References

DeFries, T. and J. Jonas (1977): Pressure dependence of NMR proton spin-lattice relaxation times and shear viscosity in liquid water in the temperature range −15–10°C. J. Chem. Phys., **66**, 896–901.

Eisenberg, D. and W. Kauzman (1969): The structure and properties of water, Oxford at the Clarendon Press, London, pp. 296.

Endo, H. (1980): Is a two-state model approach applicable to liquid water? J. Chem. Phys., **72**, 4324–4326.

Endo, H. (1982): Mechanism of the sound absorption in H_2O and D_2O liquid water. J. Chem. Phys., **76**, 4578–4589.

Endo, H. (1986): The thermodynamic consideration of $(\partial T/\partial P)_S$. (in preparation).

Endo, H. and O. Nomoto (1981): Structural absorption of ultrasonic waves in aqueous solutions of alkali halides. J. Chem. Soc. Faraday Trans. 2, **77**, 217–226.

Endo, H., A. Watanabe, and T. Fujita (1982): Sound absorption in liquid water (in Japanese). Reports of research promotion program in the National Defence Academy, **14**, 111–125.

ENDO, H. and K. SHIGEHARA (1983): Thermodynamic properties in chemical reaction processes of seawater. J. Geophys. Res., **88**, 4489–4497.
ENDO, H. and K. SHIGEHARA (1986): The pressure dependence on the adiabatic change of the temperature with pressure change. (in preparation).
FISHER, F. H. and V. P. SIMMONS (1977): Sound absorption in sea water. J. Acoust. Soc. Am., **62**, 558–564.
FRANCOIS, R. E. and G. R. GARRISON (1982): Part II: Boric acid concentration and equation for total absorption. J. Acoust. Soc. Am., **72**, 1879–1890.
JONAS, J. (1982): Nuclear magnetic resonance at high pressure. Science, **216**, 1179–1184.
KASPER, G. and K. TAMM (1980): Sound propagation at GHz frequencies in aqueous LiCl solutions. J. Chem. Phys., **72**, 5279–5280.
MELLEN, R. H., D. G. BROWNING and V. P. SIMMONS (1983): Investigation of chemical sound absorption in seawater. Part IV. J. Acoust. Soc. Am., **74**, 987–993.
PASSYNSKII, A. (1938): Compressibility and solvation of solutions of electrolytes. Acta Physicochem. U.R.S.S., **8**, 385–418.
SCHULKIN, M. and H. W. MARSH (1962): Sound absorption in sea water. J. Acoust. Soc. Am., **34**, 864–865.
STUEHR, J. and E. YEAGER (1965): The propagation of ultrasonic waves in electrolytic solutions, 351–469. Ed. by W. P. Mason, Physical Acoustics, Vol. II. Part A, Academic Press, New York-London.
WHALLEY, E. (1975): The effect of pressure on the near-neighbor distance in water. J. Chem. Phys., **63**, 5205–5207.

加圧下における海水の熱力学的性質

遠藤晴巳・重原好次
（防衛大学校）（気象庁）

すでに報告した1気圧下での海水の熱力学的性質に関する研究を概説し，加圧下における海水の熱力学的性質の平衡量 (z_0^s) を緩和量 (z_r^s) と瞬間量 (z_∞^s) に分離した．

z_0^s の圧力依存性はイオンの脱水和で説明され，水および海水の異常性は z_r^s と z_∞^s によって説明できる．この z_r^s と z_∞^s の考察をもとに，z_0^s の温度，圧力および塩分依存性は水自身の構造変化によりきまることを，また，水の構造変化に重要な役割を果すのは，海水の最主要成分の食塩であることを明らかにした．食塩水溶液の緩和機構はイオンの水和によるもののみであり，水和による過剰音波吸収量は水のそれより小さい．

The Oceanographical Magazine
Vol. 36, Nos. 1–2, pp. 17 to 24, March 1986

A method of estimating atmospheric water vapor and sea surface wind speed by the microwave radiometer of Marine Observation Satellite-1

Ichiro Isozaki
Japan Meteorological Agency
and
Akira Shibata
Meteorological Research Institute

(Received December 17, 1985; Accepted January 10, 1986)

Abstract: Two frequencies microwave scanning radiometer (MSR) is installed in the Marine Observation Satellite-1 (MOS-1) which will be launched in 1987. The main mission of MSR is to estimate total amount of water vapor and liquid water contents. But sea surface wind speed may also be estimated if the sky is clear with no clouds. In this paper, the effects of water vapor and wind on the brightness temperature observed from space are estimated by numerical simulation based on the radiosonde observations. Then the expressions of total amount of water vapor and sea surface wind speed are introduced as functions of the brightness temperature which will be observed by MSR stalled in MOS-1. The effect of sea surface temperature on the brightness temperatures of the surface at frequencies of 23.8 GHz and 31.4 GHz is also discussed. It is concluded that the effect is usually negligible but may introduce geographical bias correction to the observed brightness temperature.

1. Introduction

Marine Observation Satellite-1 (MOS-1) is the first Japanese earth observation satellite which will be launched in 1987. Two frequencies (23.8 GHz and 31.4 GHz) microwave scanning radiometer (MSR) is to be installed in MOS-1 with the main mission of observations of total amount of water vapor and liquid water contents in the atmosphere. The radiometer also senses the radiation from sea surface from which the wind speed may be estimated. As MSR has only two frequencies, more than two unknown parameters cannot be determined simultaneously from its radiation observation. Accordingly we will discuss a technique for measuring water vapor and wind speed above the sea surface in clear air conditions when no clouds exist.

2. Estimation of brightness temperature

MSR is installed in MOS-1 in the way whose antenna directs to the earth and the sky horn directs to the space. The direction of the antenna main beam is offset by 10 degrees from the nadir direction, and scans conically around the nadir direction with a period of 3.2 seconds. In the scanning period, observations are performed on the rear half circle and house keeping data for the calibration are obtained on the front half circle. Swath

Table 1. Specification of MOS-1 MSR

Frequency	23 GHz	31 GHz
RF Bandwidth	400 MHz	500 MHz
Beam width	1.99 deg.	1.45 deg.
Polarization	H or V	V or H
Integration time	10 & 47 msc	
Radiometric resolution	1.0 K at 300 K	
Dynamic range	30–300 K	
Incidence angle	11 deg.	
Swath width	312 km	

width is about 320 km. The main specifications of MSR are shown in Table 1.

Brightness temperatures observed from space, $T_B(f)$, is expressed approximately as follows,

$$T_B(f)=T_{BS}\exp(-\tau_0)+\int_0^z T(h)\alpha(h)\exp\left(-\int_h^z \alpha(h')\sec\theta\, dh'\right)\sec\theta\, dh \tag{1}$$

where $T(h)$ and $\alpha(h)$ are the atmospheric temperature and the absorption coefficient at the height h respectively, f the frequency, z the height of the satellite, θ the antenna view angle, and

$$\tau_0=\int_0^z \alpha(h)\sec\theta\, dh, \tag{2}$$

T_{BS} is the sea surface brightness temperature, where

$$T_{BS}=T_0 e_1+(1-e_1)\int_0^\infty T(h)\alpha(h)\exp\left(-\int_0^h \alpha(h')\sec\theta\, dh'\right)\sec\theta\, dh;\ i=H \text{ or } V. \tag{3}$$

T_0 is the sea surface temperature, and e_1 the sea surface emissivity. H and V are the horizontal and vertical polarization respectively.

The output from the microwave radiometer is the brightness temperature averaged over the whole solid angle weighted by the antenna pattern and is called the antenna temperature T_A,

$$T_A=\frac{1}{4\pi}\iint_{4\pi} G(\theta,\phi)T_B(\theta,\phi)\,d\Omega, \tag{4}$$

where $G(\theta,\phi)$ is the normalized antenna gain function, θ and ϕ the angles of elevation and azimuth respectively, and Ω the solid angle. Antenna receiving power P is related to the antenna temperature as follows,

$$P=kT_AB_f \tag{5}$$

where k is the Boltzman's constant and B_f the band width. Practically, antenna temperature T_A is calculated by Eq. (5) using the antenna receiving power P. Then, the brightness temperature $T_B(f)$ is obtained from T_A through the antenna pattern correction. As seen in Eqs. (1) and (3), physical parameters contributing to the variation of $T_B(f)$ are $T(h)$, $\alpha(h)$ and e_1. And e_1 is function of temperature, salinity, surface roughness and foam cover of sea water. Because the relations between $T_B(f)$ and respective parameters depend on frequency differently, each parameters can be estimated statistically from the values of $T_B(f)$ at several precisely chosen frequencies. Two frequencies of MSR are chosen to

determine an amount of water vapor and cloud water contents in the atmosphere. But the observations of brightness temperature at these frequencies from space may be used to estimate sea surface wind speed as was discussed by Wilheit (1979).

3. Simulation

3.1 Procedure of simulation

Expected values of brightness temperature $T_B(f)$ when MSR sees the ocean surface from space are estimated based on Eq. (1) by use of radiosonde data. Then the obtained $T_B(f)$ is related to the total amount of water vapor in the atmosphere and the sea surface wind speed.

In the calculation, the atmosphere is divided in horizontal layers with thickness of 0.2 km between surface and 12 km-height, and with thickness of 1 km between 12 km and 30 km-height (Shibata and Isozaki, 1985). And then no absorbing materials are assumed in the atmosphere higher than 30 km. In each atmospheric layer, pressure, temperature and humidity are assumed to be homogeneous. It is also assumed that the sea surface temperature is constant with 20°C. As will be discussed in the later section, variations of sea surface temperature cause only a little variations of sea surface brightness temperature at frequencies of 23.8 GHz and 31.4 GHz.

52 samples of radiosonde data taken under clear sky condition are selected for the present simulation from the observations at Tateno Aerological Observatory in 1983.

3.2 Atmospheric absorption coefficient

In clear sky, gaseous O_2 and H_2O are considered to be the principal absorber. According to Liebe (1981), it is represented as follows,

$$\alpha = 0.1820 f N'', \quad dB/km \tag{6}$$

where $N''(f)$ is an ensemble of various spectra of refractive absorption;

$$N''(f) = \sum (SF'')_i + N_c'', \tag{7}$$

where $(SF'')_i$ are absorption spectra of O_2 and H_2O, S the line strength, F'' the line shape function, and N_c'' the continuum. In the present simulation, Van Vleck-Weisskopf function modified by Rosenkranz (1975) is adopted for F'';

$$F'' = \left(\frac{\gamma - (\nu_0 - f)\delta}{(\nu_0 - f)^2 + \gamma^2} + \frac{\gamma - (\nu_0 + f)\delta}{(\nu_0 + f)^2 + \gamma^2} \right) \frac{f}{\nu_0}, \tag{8}$$

where ν_0 is line center frequency, γ the line width, and δ the overlap correction which are given by Liebe (1981). Here, 3 spectral lines for H_2O and 26 spectral lines for O_2 are used for the calculation of atmospheric absorption coefficient.

3.3 Sea surface brightness temperature

Emissivity of sea surface varies with salinity, temperature and surface texture. If we assume that the sea surface is in the thermal equilibrium and specular condition, then the emissivity is related to Fresnel's reflection formula as follows,

$$e_H = 1 - R_H = 1 - \left| \frac{\cos\theta - \sqrt{\varepsilon - \sin^2\theta}}{\cos\theta + \sqrt{\varepsilon - \sin^2\theta}} \right|^2 \tag{9a}$$

$$e_V = 1 - R_V = 1 - \left| \frac{\varepsilon\cos\theta - \sqrt{\varepsilon - \sin^2\theta}}{\varepsilon\cos\theta + \sqrt{\varepsilon - \sin^2\theta}} \right|^2 \tag{9b}$$

where R is the Fresnel's reflection coefficient, and suffix H and V represent horizontal and vertical polarization respectively. ε is the complex dielectric constnat of sea water which is calculated at any frequency within the microwave band from the expression of DEBYE (1941);

$$\varepsilon = \varepsilon_\infty + \frac{\varepsilon_s - \varepsilon_\infty}{1 + i\omega\tau} - i\frac{\sigma}{\omega\varepsilon_0}, \tag{10}$$

where $\omega = 2\pi f$ is the angular frequency with f in Hz, ε_∞ is the permissivity at very high frequencies, τ is the relaxation time in second, σ is ionic conductivity in mhos m^{-1}, and $\varepsilon_0 = 8.854\ 10^{-12}$ is the permissivity of free space in farad m^{-1}. The quantities ε_s, τ and σ are all functions of the temperature and salinity of sea water. Specific values of these quantities can be calculated by substituting given values of temperature and salinity into the regression equation refined by KLEIN and SWIFT (1977).

It is confirmed by observations that the sea surface brightness temperature increases with wind speed when the sea surface is roughened by the wind. Although several theoretical models have been proposed to explain the incraese of the brightness temperature, empirical results have been widely accepted. Fig. 1 is an example summarized by WEBSTER *et al.* (1976). In this figure, the rate of increase of brightness temperature with increasing wind speed in the horizontal polarization is larger than in the nadir, and reverse is the case in the vertical polarization.

As the view angle of MSR is 10 degrees to the nadir direction, the wind effect differs

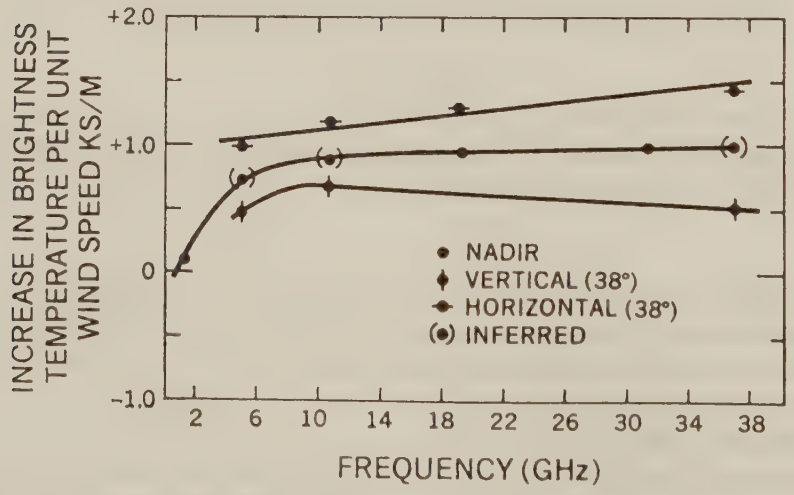

Fig. 1. Spectrum of increase in brightness temperature caused by wind at the ocean surface (after WEBSTER, *et al.* (1976)).

a little between horizontal and vertical polarizations and seems to have almost the same contribution to the sea surface brightness temperature as in the ease of nadir viewing. Accordingly, in the simulation, wind effect on the variation of sea surface brightness temperature is taken into considerations as follows: at first, sea surface brightness temperature is calculated based on Eq. (3), next, the obtained nrightness temperature is increased with increasing surface wind speed at the ratio of 1 K/(m/s) referring Fig. 1, then the value is transmitted to space by Eq. (1) through the atmospheric opacity.

4. Results

52 samples of brightness temperature obtained through the procedures shown in the previous section are related to the respective total amount of water vapor in Fig. 2. The difference of brightness temperature between horizontal and vertical polarizations is small and usually smaller than 3 K because the antenna view angle of MSR is near nadir. Accordingly, the brightness temperature of horizontal polarization is used in the present discussion as a matter of convenience. In Fig. 2, estimated brightness temperatures have

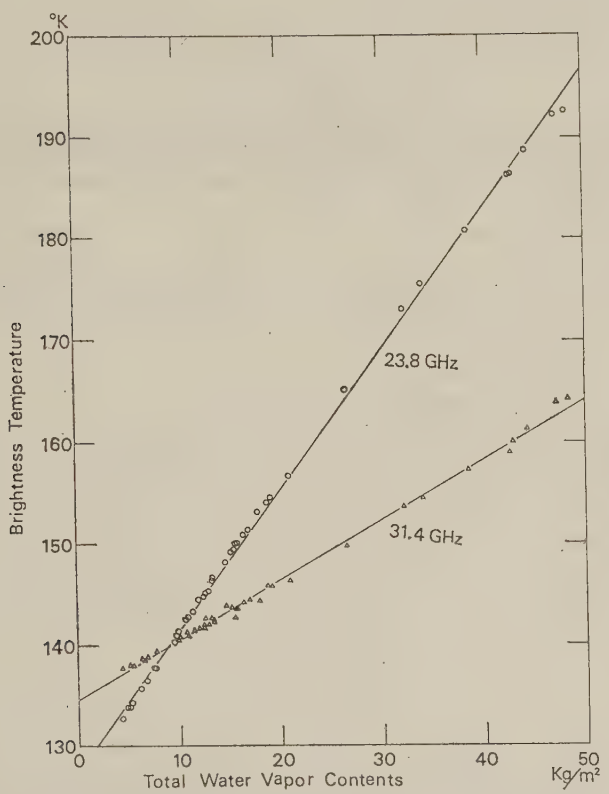

Fig. 2. Calculated brightness temperature versus total water vapor contents by use of radiosonde data at Tateno under clear sky condition.

linear relations to the values of total amount of water vapor without regard to their vertical profiles. The relations are

$$T_{B23H}=127.55+1.38\rho \quad (11a)$$

$$T_{B31H}=134.61+0.54\rho \quad (11b)$$

where T_{B23H} and T_{B31H} are the brightness temperature of horizontal polarization of 23.8 GHz and 31.4GHz respectively and ρ the total amount of water vapor in Kg/m^2. The frequency 23.8 GHz is near the water vapor absorption line of 22.2 GHz, and 31.4 GHz is in the window region between two water vapor absorption lines of 22.2 GHz and 67.8 GHz. So the effect of water vapor on the variation of brightness temperature of 23.8 GHz is 2.5 times as large as that of 31.4 GHz.

Wind effect to the brightness temperature is also estimated using the same 52 samples of radiosonde observations with the procedures mentioned in the previous section. The estimated quantities are related to the total amount of water vapor respectively in Fig. 3. In this figure, the wind effect on the variation of brightness temperature becomes small than the values on the sea surface, and the reduction of the wind effect becomes notable linearly with increase of water vapor. Moreover, the reduction at 23.8 GHz is about 2.6 times as large as that at 31.4 GHz because of the spectral characteristics of atmospheric opacity due to water vapor. The relations in the figure are as follows,

$$r_{23H}=0.98-0.0046\rho \quad (12a)$$

$$r_{31H}=0.972-0.0018\rho \quad (12b)$$

where r_{23H} and r_{31H} are the increasing ratios of horizontally polarized brightness temperature of 23.8 GHz and 31.4 GHz to the increase of wind speed respectively.

From Eqs. (11) and (12)

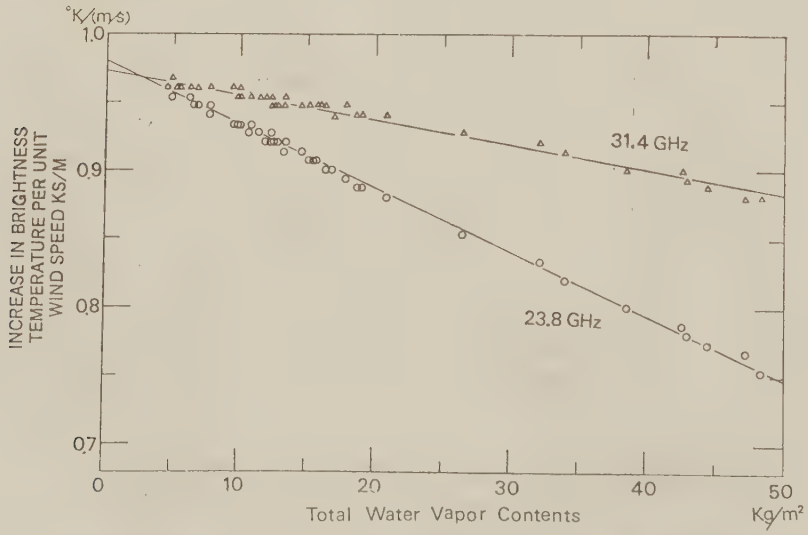

Fig. 3. Reduction of the wind effect on brightness temperature due to the increase of water vapor content in the atmosphere.

$$T_{B23H}=127.55+1.38\rho+(0.98-0.0046\rho)W \tag{13a}$$

$$T_{B31H}=134.61+0.54\rho+(0.972-0.0018\rho)W \tag{13b}$$

where W is the sea surface wind speed in m/s.

Now, putting

$$T_{23}=T_{B23H}-127.55$$

$$T_{31}=T_{B31H}-134.61$$

then, from Eq. (13)

$$\rho=\frac{0.972T_{23}-0.98T_{31}}{0.8126+0.0018T_{23}-0.0046T_{31}} \tag{14}$$

$$W=1.6993T_{31}-0.6649T_{23} \tag{15}$$

These are the resulting equations which are used to estimate total amount of water vapor and sea surface wind speed in the clear air condition from the brightness temperatures which will be observed by MSR of MOS-1.

5. Concluding remarks

In this paper, the effects of water vapor and wind speed on the brightness temperature observed from space are estimated by numerical simulations. Then the expressions of total amount of water vapor and sea surface wind speed are introduced as functions of the brightness temperature which will be observed by MSR stalled in MOS-1. Practically, the numerical constants contained in the resulting equations may be modified by use of observations made by MSR after the launch of MOS-1, because actual observations of brightness temperature contain some uncertainties of radiometric correction and antenna pattern correction.

In the present simulation sea surface temperature is assumed to be constant of 20°C. Variation of sea surface temperature affects the brightness temperature of sea surface through the first term of right hand side of Eq. (3) and the complex dielectrc constant of Eq, (10).

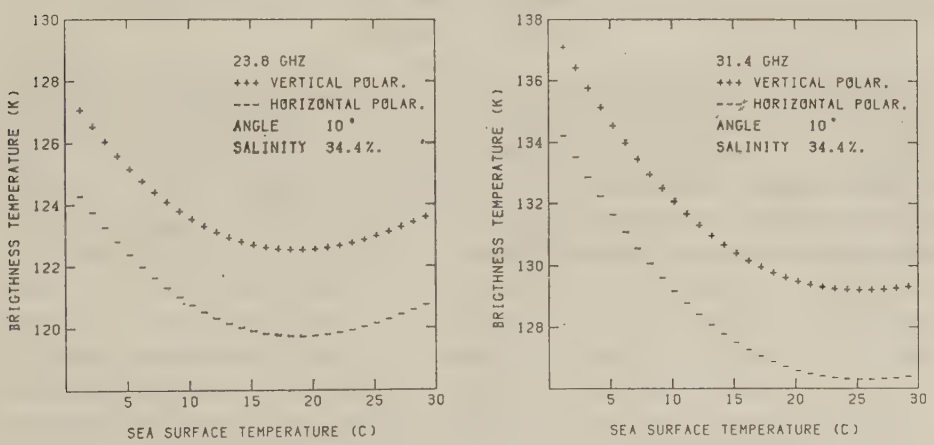

Fig. 4. Sea surface brightness temperature versus sea surface temperature, under the condition that the second term of Eq. (3) is ommited.

Figure 4 shows the brightness temperatures of sea surface which are calculated at several sea surface temperatures with constant salinity of 34.4. In this figure, the brightness temperature varies only within 1 K when sea surface temperature varies between 15°C and 30°C. But, when sea surface temperature decreases below 15°C, brightness temperature increases about 0.4 K with the decrease of sea surface temperature of 1°C. Anyway, the effect of the variation of sea surface temperature on the brightness temperature which will be observed by MSR of MOS-1 is usually neglected because the sea surface temperature varies gradually and is small. But local bias corrections will be necessary to adjust to the geographical distribution of sea surface temperature.

References

DEBYE, P. (1929): Polar Molecules, Dover Reprint, originally pub. Reinhold Publishing Corp., 1929; see also K. S. COLE and R. H. COLE, "Dispersion and absorption in dielectrics," J. Chem Phys., **9**, 341–351, 1941.

KLEIN, L. A. and C. T. SWIFT (1977): An improved model for the dielectric constant of sea water at microwave frequencies. IEEE Trans. Antennas and propag., AP-**25**, 104–111.

LIEBE, H. T. (1981): Modeling attenuation and phase of radio waves in air at frequencies below 1000 GHz. Radio Sci., **16**, 1183–1199.

ROSENKRANZ, P. W. (1975): Shape of the 5 mm oxygen band in the atmosphere. IEEE Trans. Antennas and propag., AP-**23**, 498–506.

SHIBATA, A. and I. ISOZAKI (1986): Microwave radiometer experiments at a marine observation tower, in press in Papers in Meteorology and Geophysics.

WEBSTER, W. J. Jr., T. T. WILHEIT, D. B. ROSS and P. GLOERSEN (1976): Spectral characteristics of the microwave emission from a wind driven foam cover sea. J. Geophys. Res., **81**, 3095–3099.

WILHEIT, T. T. (1969): The effect of wind on the microwave emission from the ocean's surface at 37 GHz. J. Geophy. Res., **84**, 4921–4926.

MOS-1 のマイクロ波放射計による水蒸気及び海上風速推定の一方法

磯崎一郎・柴田　彰

（気象庁）（気象研究所）

概　　要

1987年に打ち上げ予定の海洋観測衛星 (MOS-1) には2周波数のマイクロ波放射計 (MSR) が搭載される．これは水蒸気量及び雲水量の推定を目的としているが，雲が無い場合には海上風が推定できる可能性がある．この報文では，ラジオゾンデ観測に基づいたシミュレーションによって，輝度温度に及ぼす水蒸気と風の効果を見積り，それらを量的に推定する式を導いた．海面の 23.8 GHz と 31.4 GHz の輝度温度に及ぼす海面水温の効果についても検討した．この効果は通常は無視できるが，広域の観測には地理学的バイアス補正が必要である．

The Oceanographical Magazine
Vol. 36, Nos. 1–2, pp. 25 to 32, March 1986

Sea wave condition of typhoon 8506 and its prognostics in coastal area by the operational coastal wave prediction model of JMA

Masaaki TAKEUCHI
Japan Meteorological Agency

(Received December 18, 1985; Accepted January 16, 1986)

Abstract: Typhoon 8506 hit Shizuoka Prefecture on 1st July 1985 bringing severe storm seas along the coast of Japan, and several coastal facilities were damaged by break waters on the coast of Kanto District. The significant wave height of 9.93 m was observed at Irozaki. The present paper describes the wave conditions caused by typhoon 8506 and its geographical characteristics using analyses of synoptic ocean wave chart and wave observations with coastal wave-recorders and a drifting buoy, and makes its prognostics by the operational coastal wave prediction model of JMA. The prognostics coincide with the observations reasonably well.

1. Introduction

Typhoon 8506 IRMA was generated over the Caroline Islands on 25 June 1985, and progressed toward north along the 130°E longitude-line, with maintaining severe rainstorm and powers of the moderate scale (Fig. 1). After changing the direction to northeast over the eastern sea of Okinawa, she hit Shizuoka Prefecture and ran through into Sanriku at a speed of 70 to 85 km per hour. She brought a heavy rainfall and gale over Kanto and Tohoku Districts. On the sea, a Panamanian ship (5,150 tons) was standed on Shirahama-machi, Wakayama Prefecture. We have had the typhoon which landed on the Japanese Islands after 21 months since September 1983 when typhoon 8310 hit near Nagasaki.

Proper understanding of the wave situation at coastal sea areas is very important not only for real-time information for coastal ships, leisure, fisheries etc., but also for non-real-time one for maintaining and planning of maritime structures and coastal facilities. ISOZAKI *et al.* (1976) gave detailed descriptions of the ovean waves on Sagami Bay caused by typhoon 7416, and made a quantitative analysis on the reduction in wave height due to the sheltering effect of peninsulas and islands. TAKEUCHI (1984) discussed the characteristics of high waves on the coastal area of Japan based on the records of coastal wave-recorders. In order to accomodate growing requests for wave forecast at coastal sea area, JMA (Japan Meteorological Agency) has developed a coastal wave prediction model and introduced it in routine operation since 1983 (TAKEUCHI and TAKADA, 1985).

Followings are the report on the ocean and coastal sea situations associated with the passing of typhoon 8506 and its comparison with prognostics by the coastal wave prediction model.

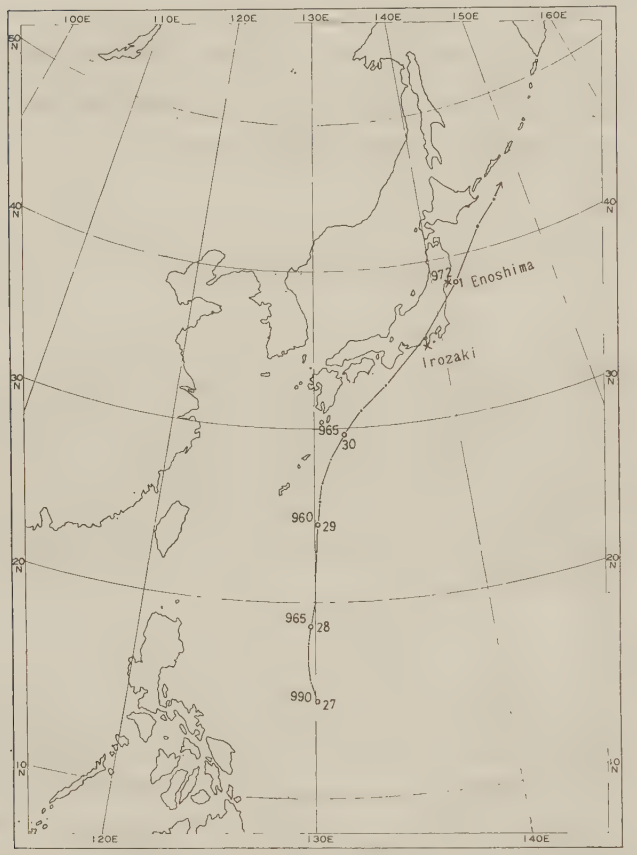

Fig. 1. Track of typhoon 8506 from 27 June to 1st July in 1985. Open circles on the track show positions of the typhoon at 0000GMT, and closed circles positions at every six hours.

2. Conditions of ocean waves

According to the analysis of sequencial ocean wave charts, sea waves began to grow significantly from 25 June, when a tropical depression developed into the typhoon scale and was named IRMA. Wave of 5 m in height was found at the center of the typhoon. Waves grew highest on 29 June, when the typhoon was located about 240 km east of Okinawa and progressing toward north along the 130°E longitude line as shown in Fig. 1. At that time wave height of 10 m was found in the southeastern sector of the typhoon. Then waves decreased gradually as the typhoon decayed with moving toward northeast.

Figure 2 shows the ocean wave analysis chart over the western North Pacific at 0000GMT 1 July issued by JMA. High wave area more than 7 m is found in the southeastern sector of the typhoon. Waves more than 3 m are distributed widely from Hokkaido to Okinawa on the Pacific Ocean, and the length of this area is about 1,200 nautical miles. While the sea is generally gentle on the Japan Sea, small high waves are locally observed under

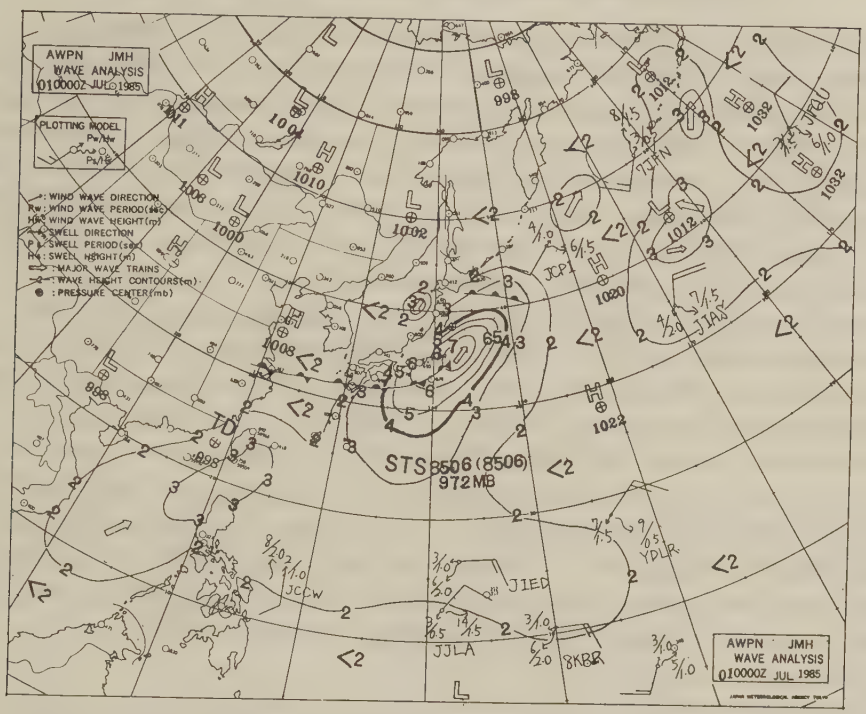

Fig. 2. Ocean wave analysis chart over the western North Pacific at 0000GMT 1st July 1985.

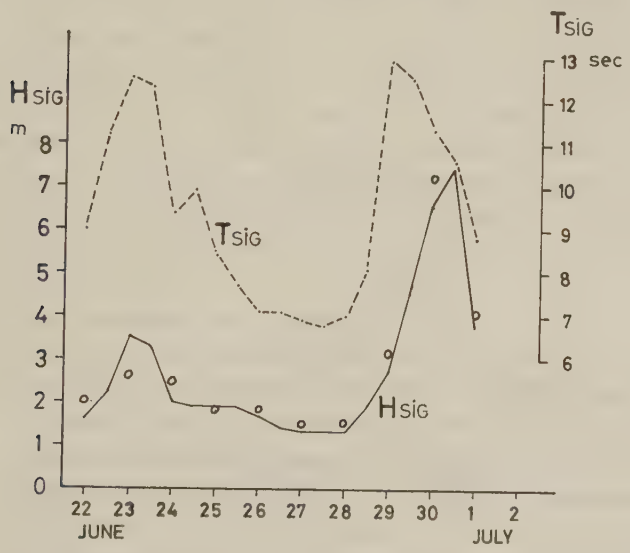

Fig. 3. Variation of Hsig (significant wave height) and Tsig (significant wave period) observed by the drifting buoy, whose location is near 30°N, 134°E.

the influence of the northeast strong winds at the western sector of the typhoon.

Japan Weather Association entrusted to Tokyo Tsushinki, Co. Ltd. the development of a drifting bouy which records the height and period of significant wave and the wave direction. A field experiment of the bouy was underway successfully when typhoon 8506 just passed by the drifting bouy. Figure 3 shows its records of Hsig (significant wave height) and Tsig (significant wave period) in every 12 hours during the period. The location of the drifting bouy moved somewhat, but the bouy was found south off Shikoku Island near 30°N, 134°E during the typhoon passed through.

Wave height began to grow from 29 June, when the typhoon was passing east of the Nanseishoto Islands, and Hsig of 7.4 m and Hmax (maximum wave height) of 13.2 m were observed at 1200GMT 30th. Long wave period at 29 June indicates a predominance of swell from the typhoon. As the typhoon approaches to the buoy, the development of wind waves overcome the swell and significant wave period Tsig decreased since 29 June. The increase of both Hsig and Tsig from 22 to 25 June is due to the swell propagating from typhoon 8505 which was generated before typhoon 8506 and progressed westward along the 18°N latitude-line. The variation of wave height obtained by the analysis of ocean wave chart is also shown in Fig. 3 by open circles. The wave heights observed by the drifting bouy correspond well with the analysis of ocean wave charts.

3. Coastal wave-recorder

JMA has equipped coastal wave-recorders at eleven stations at present (Takeuchi and Takada, 1985), the sensors of which are placed on the sea bed at a water depth of about 50 m and wave records of 20 minutes-period are taken in every three hours. Among these

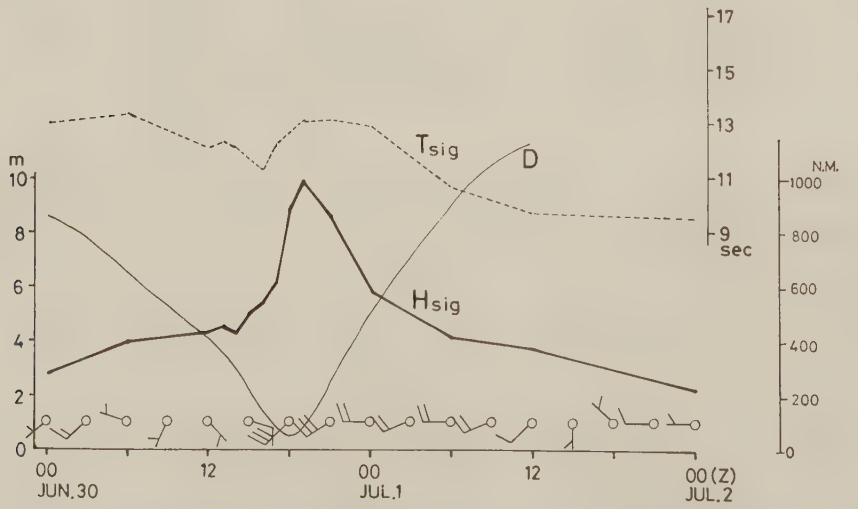

Fig. 4. Variation of Hsig and Tsig observed by the coastal wave-recorder at Irozaki, distance between the center of typhoon 8506 and Irozaki station D and wind at Irozaki Weather Station.

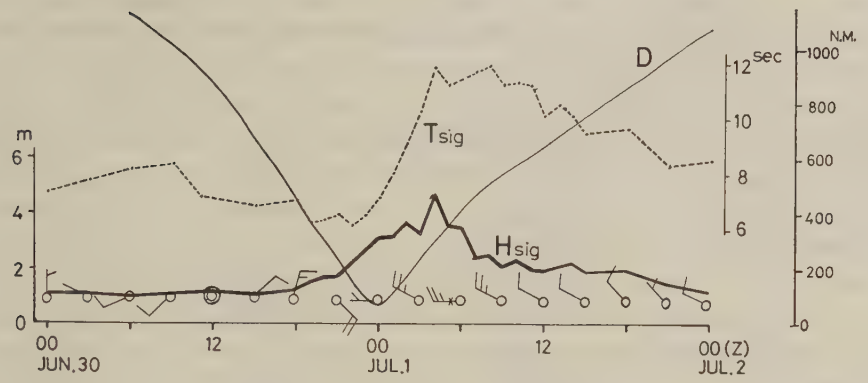

Fig. 5. Same as Fig. 4 except Enoshima.

stations, Irosaki and Enoshima stations are sited near the path of typhoon 8506 (see Fig. 1), and recorded the characteristic waves by the typhoon.

Figure 4 shows the variation of Hsig, Tsig, distance of the station from the typhoon center and wind at Irozaki during 30 June to 1st July. From 0000GMT to 1400 GMT of 30 June, wave height increases and wave period decreases gradually while the easterly wind of about 10 kt is observed at Irozaki. This is a swell propagated from southern storm area. Abrupt growth of wave height after 1500GMT 30 June is attributed directly to southwesterly gale associated with the approaching typhoon. At 1900GMT 30 June, one hour after the nearest approach of the typhoon to Irozaki, the maximum wave height of Hsig 9.93 m and Hmax 14.5 m was observed. This is the second historical record of highest waves at Irozaki station since the wave observation began in 1976.

Figure 5 shows the same factors as Fig. 4 at Enoshima. Until 2100GMT 30 June the wave height was less than 2 m and wave period 6 to 8 seconds, suffering no significant effect of typhoon 8506. The wave height and period increased gradually from 2100GMT 30th, when Enoshima entered in the storm zone, and attained to the maximum wave height of Hsig 4.58 m and Hmax 7.10 m at 0400MGT 1st July after four hours later since the typhoon approached nearest.

4. Geographical characteristics of waves

The powers of the typhoon suffered at Irozaki and Enoshima were almost the same because the time lag between the nearest approach of the typhoon to both the stations was only six hours. Nevertheless there is a great difference in the maximum wave height between the two stations, that is, the maximum Hsig at Irozaki was 9.93 and that at Enoshima was only 4.58 m. Probably this is due to the reason that Irozaki station faces to the Pacific Ocean to southward while Enoshima station opens to eastward. Furthermore, it is clear from Fig. 5 that the wave height at Enoshima continued to increase after the nearest approach of the typhoon in spite of the direction of storm wind being from land to sea. High waves at Enoshima were caused, therefore, not by the local winds but by

Table 1. Ranking of daily maximum Hsig (unit in meter) at Irozaki and Enoshima, during from Apr. 1976 to Dec. 1984 at Irozaki and from Jul. 1978 to Dec. 1984 at Enoshima.

	Enoshima		Irozaki	
Ranking	Hsig	The date of occurrance	Hsig	The date of occurrance
1	9.27	1980.12.24	10.15	1982. 8. 1
2	8.14	1980.12.25	9.02	1982. 9.12
3	7.60	1981. 8.23	8.24	1979.10.19
4	7.50	1979. 2.24	7.78	1982. 8. 2
5	7.12	1983. 2.18	6.69	1983. 8.17
6	7.10	1982.10.20	6.19	1981. 8.22
7	6.71	1984. 4.20	5.91	1983. 8.16
8	6.70	1979. 5.15	5.78	1981.10.22
9	6.61	1979. 2.25	5.55	1978. 2.28
10	6.29	1983. 2.19	5.48	1982. 9.25

Table 2. Classification of the disturbances which brought the high waves at Irozaki and Enoshima shown in Table 1.

	Disturbance	
Station	Typhoon	Cyclone
Enoshima	1	9
Irozaki	9	1

(number)

the swell arriving from the high wave area on the southeastern sector of the typhoon. High waves accompanying typhoon and extratropical cyclones usually subside as the disturbance passes away and strong winds decay. But sometimes, such as in the present case of Enoshima, high waves come lately after a passing of local storm winds because of geographical effects and the course of a disturbance.

Followings are the characteristics of high waves observed at Irozaki and Enoshima stations since the start of observations. Table 1 shows the ranking of Hsig appeared at the two stations. The average height of the top ten, based on the table, is about 7 m at both the stations. However, the wave heights scatter widely at Irozaki station in comparison with Enoshima, which suggests that there is a possibility of higher waves in future at Irozaki (TAKEUCHI, 1984). High waves at Enoshima mostly appear in winter when northwest monsoon is prevailing, while at Irozaki they concentrate in warm season. Referring to the synoptic weather chart, nine of ten high waves at Enoshima shown in Table 2 are caused by the passing of cyclones and remaining one by a typhoon. On the other hand, nine of ten high waves at Irozaki are associated with the passing of typhoons and remaining one with a cyclone. The main cause of high waves at Enoshima is quite different from Irozaki.

Consequently it is obvious that condition and process of growing high wave depend more or less on local winds and wave characteristics caused by the course of a disturbance and coastal configurations. Accordingly through knowledge and better understanding of these regional characteristics are desired for the prevention of coastal disasters.

5. Coastal wave model

JMA has developed a coastal wave model and introduced in routine operation since 1983. Wave predictions on nearly half of the coastal sea areas of Japan are put out routinely every day (TAKEUCHI and TAKADA, 1985). Figure 6 shows the coastal wave chart calculated by the model off the southern coast of Kanto District at 1800GMT 30 June, when the typhoon 8506 is just on Shizuoka Prefecture. High wave area more than 9 m is seen near the southern boundary where south to southwest gale prevails. Waves traveling to the coast from off shore subsides under the influence of geographical features, and presents a complex pattern. Relatively low waves are seen on the rear side of islands.

Figure 7 shows a comparison of Hsig between observations by coastal wave-recorder at Irozaki and estimations at the grid point corresponding to the location of Irozaki station calculated by the coastal wave model. Observations are shown by thin line labeled by OBS and estimations by thick line labeled by MODEL, where thick solid line shows hindcast and thick dotted line the 36 hours prognostic made in routine operation based on 1200GMT 30 June. Each value is plotted in every six hours since 0000GMT 30 June.

Apart from a fact that the model at 1200GMT 30 June estimates 2 m higher than the observations, the prognostic after 1800GMT nearly coincide with the observations. It is especially important to estimate maximum wave precisely for the prevention of coastal disasters. The wave height of 8.9 m was observed in coastal wave-recorder at 1800GMT 30th, and at the same time the prognostic was 8.2 m. This result means that our coastal wave model is reliable and useful to estimate the maximum design wave height.

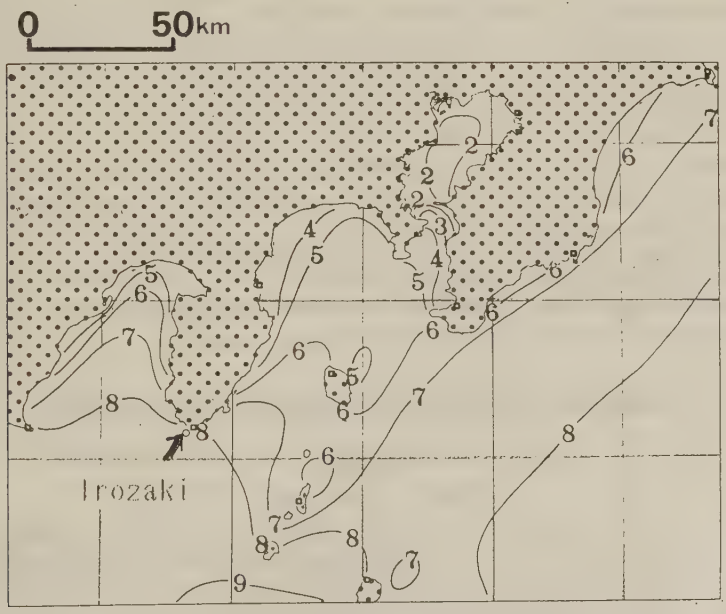

Fig. 6. Wave height distribution calculated by the coastal wave model off the southern coast of Kanto District at 1800GMT 30 June.

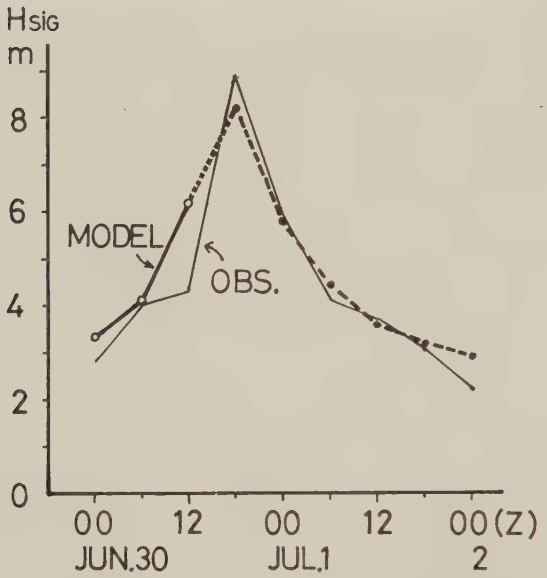

Fig. 7. Comparison between observations of the coastal wave-recorder at Irozaki and estimations by the coastal wave model.

Acknowledgements

The author would like to express thanks to Drs. I. Isozaki and M. Hatori who read the manuscript carefully and gave him useful suggestions. Also, the author thanks to the staff of Observation Division of Sendai District Meteorological Observatory and of Technical Division of Shizuoka Local Meteorological Observatory for collecting the data of the coastal wave-recorders.

References

Isozaki, I., T. Uji, T. Seto and A. Kaietsu (1976): Ocean waves on Sagami bay caused by typhoon 7416. Oceanogr. Mag., **27**, (1–2), 1–23.

Takeuchi, M. (1984): Statistical analysis of wave data obtained by the ultrasonic wave-recorder (in Japanese). Weather Service Bull., **51**(3), 179–194.

Takeuchi, M. and M. Takada (1985): Development of the operational wave forecast model in coastal area. Oceanogr. Mag., **35** (1–2), 1–20.

台風8506における波浪と数値波浪モデルとの比較

竹内昌明

（気象庁　海洋気象部）

台風8506は，1985年6月30日深夜静岡県に上陸し，関東及び東北地方を縦断し三陸海上に駆けぬけた．台風通過に伴い海上は大しけとなり，石廊崎の沿岸波浪計では 9.93 m の高波を観測し，関東地方の沿岸海域で防波堤の破損事故等沿岸施設に被害を及ぼした．

ここでは，外洋波浪図，沿岸波浪計及び漂流ブイの記録をもとに，台風による波浪の状況及び地域特性について調査した．沿岸波浪予報モデルによる波浪の推算値は観測値と良く一致していた．

The Oceanographical Magazine
Vol. 36, Nos. 1–2, pp. 33 to 42, March 1986

Distributions of floating tars and petroleum hydrocarbons at the surface in the western North Pacific

Sukeyoshi TAKATANI, Takeshi SAGI and Masanao IMAI
Japan Meteorological Agency

(Received October 7, 1985; Accepted January 17, 1986)

Abstract: The surface distributions as well as the seasonal variations of floating tars and petroleum hydrocarbons have been investigated in the seas adjacent of Japan and in the western North Pacific since 1977. The Kuroshio and its counter current south of Japan are extensively polluted with floating tars being 0.24 mg/m² in the mean. The Japan Sea is contaminated with floating tars being 0.21 mg/m² in the mean. While floating tars are only 0.004 mg/m² in the mean in the south of Equatorial Counter current.

Floating tars are high in summer and low in winter at the sea surface south of Japan. It is seen that floating tars is transported to the south by the north-west monsoon prevailing in winter. From 1981 floating tars remarkably decrease in occurrence in the areas investigated.

The mean concentration in petroleum hydrocarbons larger than 250 ng chr./kg occur at each station of PH-1 and PH-6 east of Japan. The Kuroshio region is rather low in polluted level of petroleum hydrocarbons. The trend of increasing of petroleum hydrocarbons in winter appears in most of the regions. It is also seen that petroleum hydrocarbons decrease gradually year by year.

1. Introduction

In responce to the request of the Marine Pollution (petroleum) Monitoring Network (MARPOLMON) of IGOSS, The Japan Meteorological Agency has started on the monitoring of floating tars and petroleum hydrocarbons at the surface in the western North Pacific since 1977. On the basis of the data obtained by the Japan Meteorological Agency. SANO *et al.* (1979) and SHIGEHARA *et al.* (1979) reported preliminary on floating tars and petroleum hydrocarbons at the surface in the western North Pacific, respectively. SUZUOKI and MATSUZAKI (1983) also pointed out that floating tars were distributed heterogeneously and relatively enriched at some stations depending on the dynamics of the surface water.

The present study is carried out to clarify the seasonal, the annual and the regional variations on floating tars and on petroleum hydrocarbons at the surface in the western Norht Pacific.

2. Materials and methods

The surveys have been done four times a year in the sea adjacent of Japan and twice a year in the western North Pacific by using the network of sampling stations with purpose of monitoring the longterm variation of pollutants and relevant oceanographic parameters.

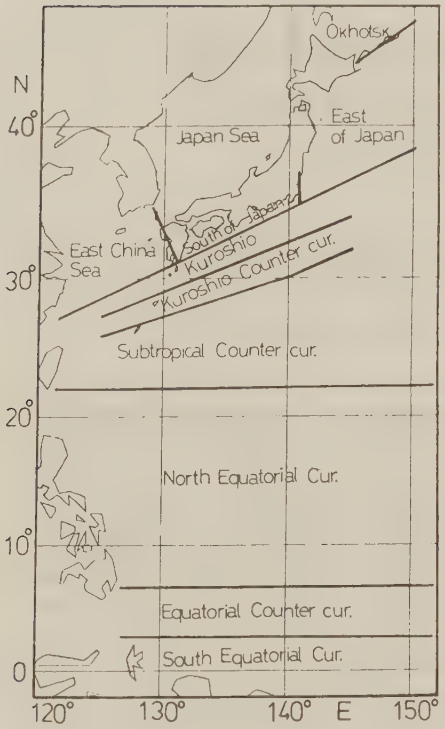

Fig. 1.

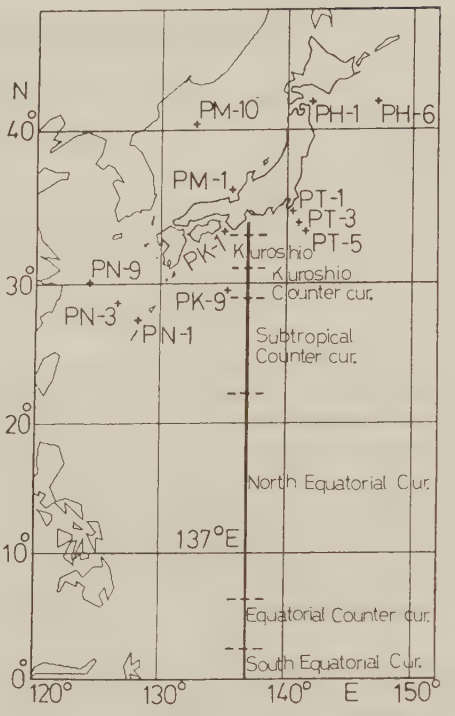

Fig. 2.

Fig. 1. Names of sea areas referred to the present study.
Fig. 2. Fixed stations around Japan and fixed line along 137°E on sampling of petroleum hydrocarbons.

823 and 912 samples were obtained respectively during the cruises in summer 1977 to summer 1985 on floating tars and during the cruises in winter 1977 to autumn 1984 on petroleum hydrocarbons. Samplings have been carried out usually in a day-time on floating tars and at the fixed stations around Japan and fixed line at 137°E on petroleum hydrocarbons. As for petroleum hydrocarbons, 674 samples were collected at the fixed stations around Japan and fixed line at 137°E (refer to Fig. 2).

Names of sea areas referred to the present study are shown in Fig. 1.

The method of sampling and measurement for floating tars at the surface were explained previously by SANO et al. (1979). The concentration is given as net weight of tars (mg) per unit sea surface area (m^2).

The fluorescence spectro-photometry using a carbon tetrachloride extraction for determination of dissolved and/or dispersed petroleum hydrocarbons in the surface water was described in detail by SHIGEHARA et al. (1979). The concentration of petroleum hydrocarbons is converted into chrysene equivalent.

3. Results

3.1 Distribution of floating tars

The geographical distribution of floating tars filling with all data are presented in Fig. 3. As shown in the figure, floating tars are abundant in the seas adjacent of Japan, especially in the Kuroshio and its counter current. It is also seen that floating tars are transported to the south in winter monsoon season in the sea south of Japan.

The frequency distribution classified by the logarithmic concentration and the mean concentration of floating tars are shown in Fig. 4 in each of regions. When the mean

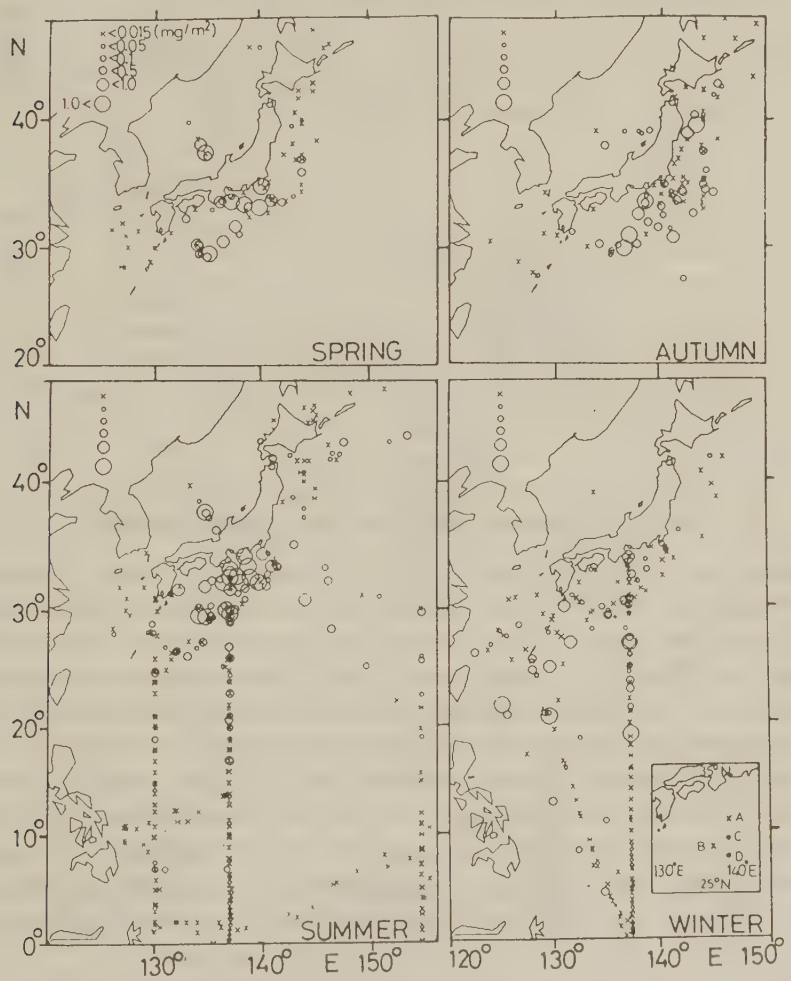

Fig. 3. Distribution of floating tars (1977–1985). Lower right box in the figure shows the average centers of floating tars concentration; A in summer and B in winter, respectively.

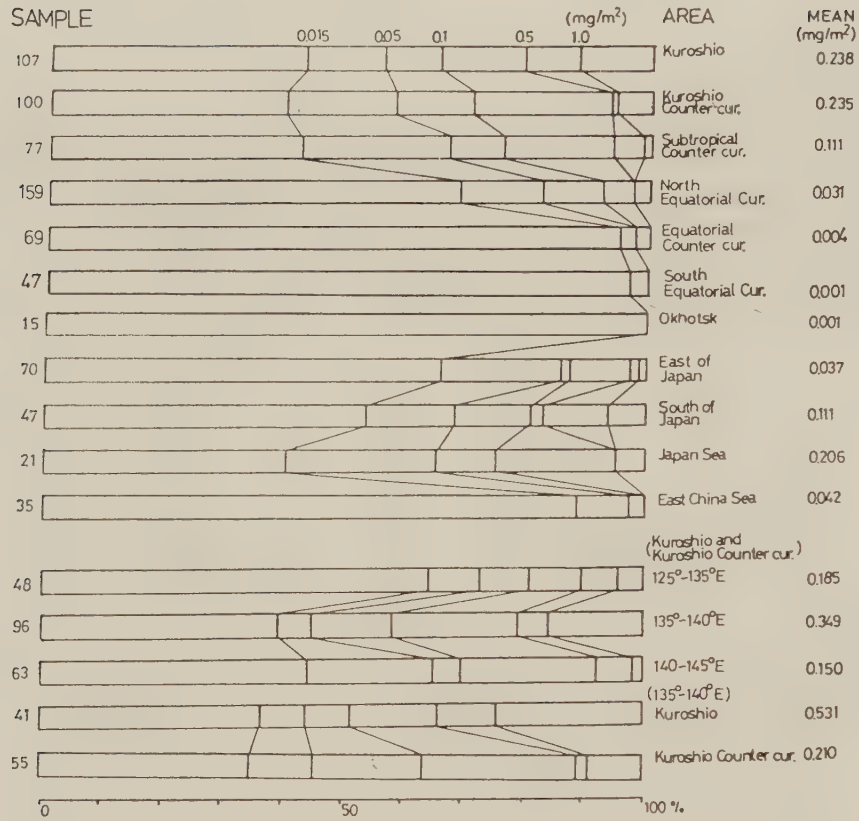

Fig. 4. Frequency distribution classified by the logarithmic concentration and the mean concentration of floating tars in each of sea regions.

concentrations were calculated, values larger than 5 mg/m² were counted out in order to represent the general feature. In the Kuroshio regions, floating tars concentrations larger than 0.5 mg/m² occur at the stations of about 20% in the whole, and floating tars concentrations larger than 0.05 mg/m² amount to 45%. The mean concentration is 0.24 mg/m² in the Kuroshio. While at the surface south of Equatorial Counter current, floating tars concentrations smaller than 0.015 mg/m² amount to more than 90% in the whole. There were no floating tars concentrations larger than 0.5 mg/m². The mean concentration is only 0.001 mg/m² at the surface in the South Equatorial Current. These findings indicate that the surface in the Kuroshio regions is extensively polluted with floating tars.

It should be noted that the surface in the Japan Sea is contaminated with floating tars next to the Kuroshio regions. The surfaces east of Japan and in the East China Sea are relatively low polluted and in the Okhotsk Sea there is no floating tars.

The longitudinal distribution of floating tars from west to east in the Kuroshio and its counter current are shown in the lower part of Fig. 4. The sea area of 135°E–140°E shows the highest pollution with floating tars. There exist many traffic routes of maritime

transportation including huge tankers toward industrial zones near Tokyo and Osaka. Various kinds of wastes with petroleum origin are possibly discharged into marine environment.

3.2 Distribution of petroleum hydrocarbons

Concerning petroleum hydrocarbons at the surface, Fig. 5 shows the mean concentration in each of fixed stations around Japan and in each of current systems at 137°E. In order to represent the general feature, the values larger than 1000 ng chr./kg were counted out of the mean concentration.

At the surface in the North Equatorial Current and the Equatorial Counter current, petroleum hydrocarbons are relatively little, and an increase towards the coast of Japan is not clear in contrast with floating tars. High concentrations in petroleum hydrocarbons larger than 200 ng chr./kg appear at the stations (PH-1, PH-6) in the area east of Japan and at a station (PK-9) in the sea south of Japan.

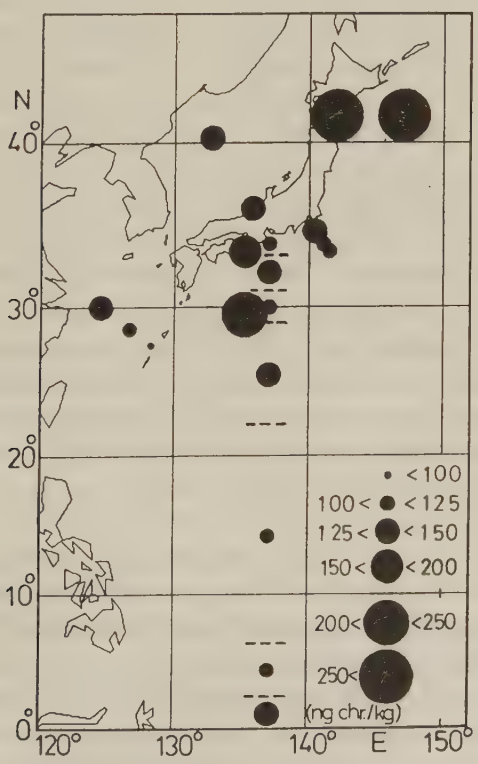

Fig. 5. The mean concentration of petroleum hydrocarbons (1977–1984) in each of fixed stations around Japan and in each of current system in the fixed line at 137°E.

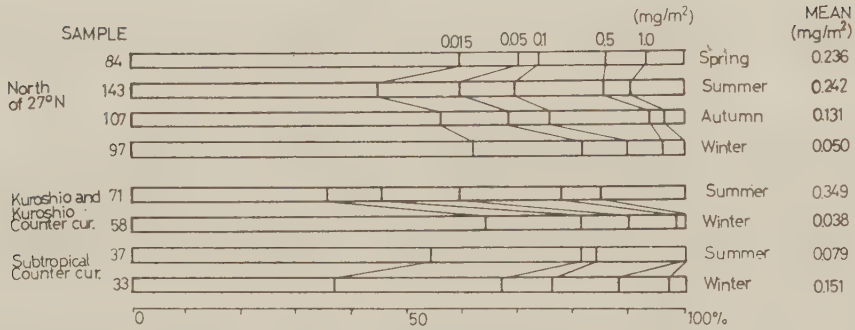

Fig. 6. Frequency distribution classified by the logarithmic concentration and the mean concentration of floating tars at each season.

3.3 Seasonal variation of oil pollution and affection by wind system

The frequency distribution classified by the logarithmic concentration and the mean concentration of floaring tars in the waters north of 27°N are shown in Fig. 6 at every season. This figure leads to the followings: floating tars increase in spring, reach the highest value in summer and decrease in autumn. The amount of tars in winter is only one fifth as compared with the one in summer. This seasonal variation is much indebted to the high value in summer and the low value in winter in the regions of the Kuroshio and its counter current. While the surface in the Subtropical Counter current in winter shows twice as much as the concentration in summer.

As shown in the lower right part of Fig. 3, in the area at 25°N–35°N and 130°E–140°E, the weighted average center of floating tars distribution comes to the point A in summer and point B in winter, respectively. Now assuming that the average center of floating tars in winter is located at point A, the Ekman flow by the monsoon wind system was calculated at point A. On the basis of the data of Ship Research Institute (1980), the mean wind speed in this region in winter was about 16 knots. And the average wind considering the frequency of appearance about direction of the wind is northwest wind and its speed is about 7 knots. For calculation, next formula was used.

$$V=0.0126W/\sqrt{\sin Q}$$

(V: Ekman flow speed m/s W: Wind speed m/s Q:latitude)

The north-west wind of 7 knots makes the Ekman flow whose direction is the south and the speed is about 0.064 m/s. This Ekman transportation make the average location of floating tars move from point A to point C and further point D after one month and two months, respectively. These points C and D coinside approximately with the point B where is average center of floating tars in winter.

As the result of above considerations, it can be said that the transportation by the wind system in winter have an effect on the distribution of floating tars. From the same point of view, an increase of floating tars from spring to summer in the sea southward of Japan seems to be caused by the Ekman transportation by the south-east monsoon in summer.

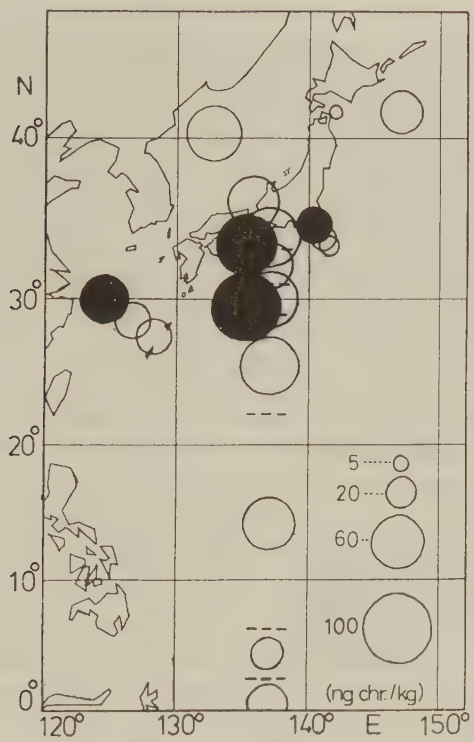

Fig. 7. The difference between mean concentration of petroleum hydrocarbons in winter and that in summer in each of fixed stations around Japan and in each of current systems at 137°E. Open circle shows that the mean concentration in winter is larger than that in summer.

Figure 7 shows the difference between mean concentration of petroleum hydrocarbons in winter and that in summer. Open circle shows that the mean concentration in winter is larger than that in summer. Though the seasonal variation is not too much clear. petroleum hydrocarbons in winter are larger than those in summer in most of the regions. However, the concentrations are higher in summer than in winter in some stations south of Japan and in the East China Sea, where their mean concentration is high compared with surrounding stations.

3.4 Year to year variation of oil pollution

The frequency distribution classified by logarithmic concentration of floating tars are shown in Fig. 8 in annual order. The figure shows the peak in floating tars in 1980. This is because of small number of data during 1977 and 1979 in the adjacent seas of Japan where show relatively high contamination with floating tars. From 1981 floating tars decrease distinctly year by year. In 1984, a higher contamination more than 0.5 mg/m^2 is not detected and the values less than 0.015 mg/m^2 in occurrence amount to 90% of all data. This decrease in floating tars is especially indebted to the decrease in the regions

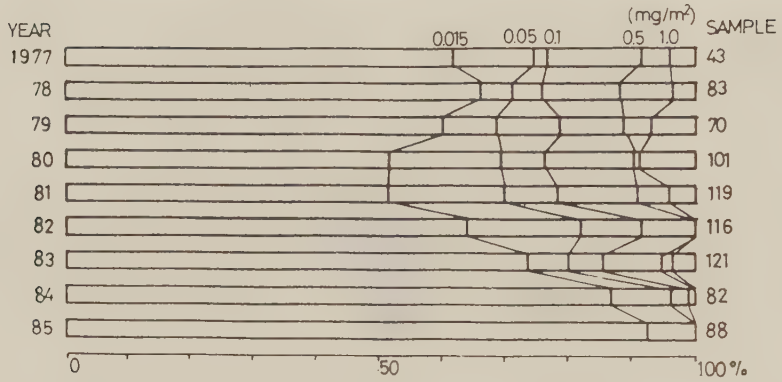

Fig. 8. Frequency distribution classified by the logarithmic concentration of floating tars in annual order.

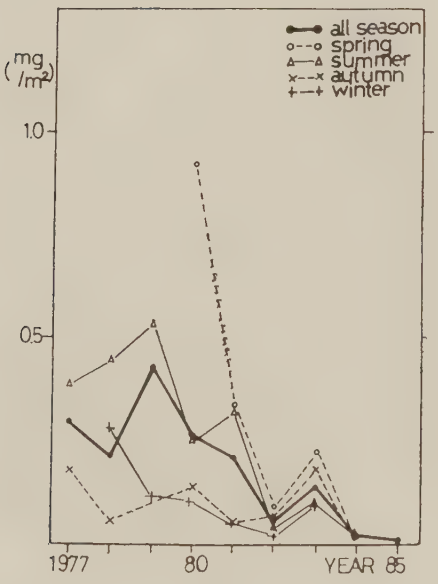

Fig. 9.

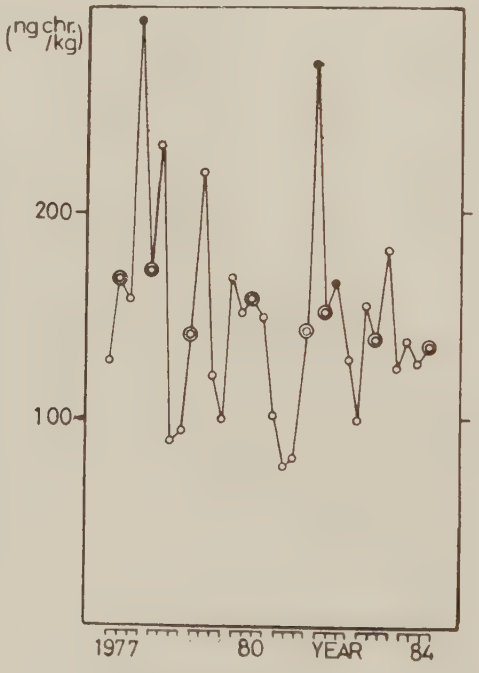

Fig. 10.

Fig. 9. Year to year variation of the mean concentration of floating tars in the regions north of 20°N.

Fig. 10. Year to year variation of the mean concentration of petroleum hydrocarbons in each season in the regions north of 20°N.

of the Kuroshio and its counter current.

Year to year variations of the average concentration of floating tars in the regions north of 20°N are shown in Fig. 9. The average concentration of floating tars decreases re-

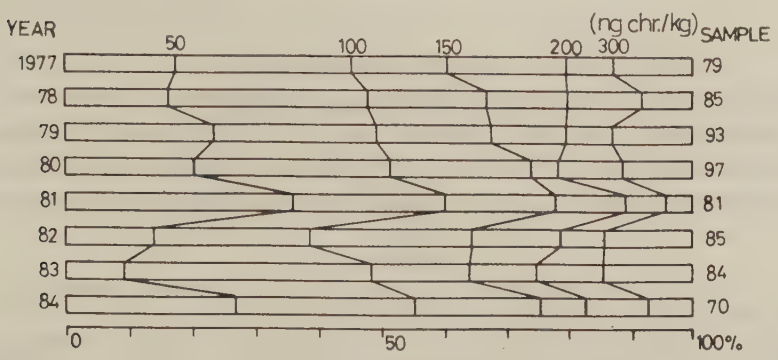

Fig. 11. Frequency distribution by the logarithmic concentration of petroleum hydrocarbons in annual order.

markably from 1979 (0.421 mg/m²) to 1984 (0.015 mg/m²) owing to the decrease mainly in spring and in summer. While the values larger than 5 mg/m² are counted out of the mean value in this paper, such a high value is found only for one sample in each year before 1981. Up to now, the maximal concentration of 24.2 mg/m² occurred in winter 1978.

As concerns petroleum hydrocarbons, the frequency distribution classified by the logarithmic concentration is shown in Fig. 11 in annual order. It appears that petroleum hydrocarbons within the each range lower than 150 ng chr./kg show a slight yearly increase. Time variation of the seasonal mean concentration is shown in Fig. 10. In this figure double circle shows the value of samples whose mean concentrations are larger than 120 ng chr./kg and standard deviations are smaller than 120 ng chr./kg. It seems that petroleum hydrocarbons decrease slightly year by year since 1977.

4. Conclusion

As for the concentrations of floating tars and petroleum hydrocarbons, its distribution and seasonal and year to year variations are investigated. However, precise correlation is not found between floating tars and petroleum hydrocarbons on the distribution and also on the seasonal variations. It may suggest that their source and behavior in the marine environment are different.

The sea areas of 135°E–140°E in the Kuroshio and its counter current show the highest pollution with floating tars. In those areas, since the average location of the pollutant concentration is drifted toward south in winter, it can safely be said that the distribution of floating tars in winter is affected by the monsoon wind system.

Floating tars remarkably decrease since 1981. Further, most of floating tars collected in recent years seem to be long aged in external appearance after discharge to the marine environment. However, the surface in the adjacent seas of Japan show still higher contamination of oil pollution as compared with the surface in the southern region of the North Equatorial Current. The monitoring of floating tars and petroleum hydrocarbons at the surface in the western North Pacific is ongoing by the Japan Meteolorogical Agency to get further information of oil pollution.

Acknowledgements

The authors wish to acknowledge members of Oceanographical Division and crew of the R/V Ryofu Maru, Kofu Maru, Shumpu Maru, Chofu Maru and Seifu Maru of the Japan Meteorological Agency for their help in collection of sample in this survey. They also wish to acknowledge Mr. A. SANO of Oceanographical Division for his helpful advice.

References

SANO, A., N. SATO and N. KUBO (1979): Floating particulate petroleum residues, tar ball, in the western Pacific. Oceanogr. Mag., **30**, 47–54.

SHIGEHARA, K., K. KIMURA, J. OHOYAMA and N. KUBO (1979): Fluorescing materials in marine environment and petroleum pollution. Oceanogr. Mag., **30**, 61–74.

Ship Research Institute (1980): Papers of Ship Research Institute Supplement No. **3**, 123.

SUZUOKI, T. and M. MATSUZAKI (1983): Tar ball distribution and dynamics of surface waters in the western North Pacific. Oceanogr. Mag., **33**, 19–26.

北西太平洋域における浮遊油塊と油分の分布

高谷祐吉・驚　猛・今井正直

（気象庁）

気象庁では1977年以来，日本周辺海域と北西太平洋域で，浮遊油塊と油分の観測を実施している．ここでは，海洋気象部のみならず函館・神戸・長崎・舞鶴海洋気象台が観測した資料を一括して，水平分布と季節・経年変動を解析してみた．

浮遊油塊は日本南方の黒潮とその反流域で多く1977～1985年の平均値が 0.24 mg/m² であり，とくに 135°～140°E 間で 0.35 mg/m² に達している．日本海も多く 0.21 mg/m² である．赤道反流以南では少なく 0.004 mg/m² であり，オホーツク海では 0.001 mg/m² にすぎない．浮遊油塊は夏季には黒潮とその反流域に分布の中心があり，冬季になると南方の亜熱帯反流域に移動する傾向がある．これは冬季の季節風の影響によるものであることをエクマンの理論を用いて説明した．なお，1981年以後，浮遊油塊は著しく減少している．

油分の平均濃度（1977～1984：）は，北海道南方で高く 250 ng chr./kg であり，黒潮とその反流域ではこれより低く，北赤道海流域では 100 ng chr./kg にしかすぎない．油分濃度の季節変化は明瞭ではないが，夏季よりも冬季が高い海域が多い．油分も徐々にではあるが，経年的に減少傾向を示している．

The Oceanographical Magazine
Vol. 36, Nos. 1–2, pp. 43 to 49, March 1986

Preliminary study on sinking particles in the adjacent seas of Tokyo

Yuji KANO
Japan Meteorological Agency

(Received November 26, 1985; Accepted January 14, 1986)

Abstract: It is possible that pollutant matters from land water to sea water are removed from the upper layer biochemically before reaching the Kuroshio which may have large capacity to transport and diffuse the various matters in sea water. In order to study the possibilities of change and removal of pollutant matters, the apparatus to collect the sinking particle in sea water (sediment trap) are developed as a simple system for easy treatment on board. The sediment trap systems are set up four times from October 1983 to October 1984 in the adjacent sea of Tokyo (Sagami Bay, Suruga Bay and near Niijima) by R.V. Ryofu Maru which belongs to the Japan Meteorological Agency (JMA). Phosphorus and plant pigments contained in the collected sinking particle in the traps are analyzed. From the four observations it is revealed that in Sagami Bay the sinking flux of phosphorus is the largest in autumn but varies little with depth. From the observation in October 1984 it is revealed that the fluxes of phosphorus and plant pigments in Sagami Bay and in Suruga Bay are both large but the difference between the two is small. On the other hand the fluxes of phosphorus and plant pigments near Niijima are smaller than those in Sagami Bay and Suruga Bay. The fact of large regional variation shows that phosphorus loaded from land water is removed before reaching the Kuroshio. This study is supported by the Self-Purification Project which JMA is charged with, in the Kuroshio Exploitation and Utilization Research Program (KER) promoted by the Science and Technology Agency of Japan.

1. Introduction

Sediment Trap studies have shown that the sinking particle plays an important role in removing the various pollutant matters from the surface layer to the deep ocean. But sediment trap experiment in offshore region has had technical difficulties in determining the accurate location for retrieval of the system and in the releasing mechanism under high water pressure. Recent rapid progress in electronics has dissolved such problems. Many papers report analytical results on sediment trap studies (N. FUJITA and S. NISHIZAWA (1979), G.A. KNAUER and J.H. MARTIN (1981), K. ISEKI (1981), D.M. KARL and G.A. KNAUER (1984) and S. NORIKI *et al.* (1985)).

Marine Department of the Japan Meteorological Agency (JMA) is charged with the Self-Purification Project in the Kuroshio Exploitation and Utilization Research Program (KER) promoted by the Science and Technology Agency of Japan. In this project under which the present work is carried out. not only large capacities of the Kuroshio for transport and diffusion of the pollutant matters but also biochemical changes of the pollutant matters are the important subjects of the study (JMA, 1985). The pollutant matters loaded from land water may be changed to particulate forms biochemically and may be moved

to deep water or sea floor in coastal region before mixed or diffused into the Kuroshio, which is expected to transport a large amount of pollutant matters to the wide area of the ocean.

The sinking particles in the adjacent region of Tokyo are collected by using the same type sediment traps several times a year. The phosphorus and the plant pigments content in the particulate matter are analyzed. This report describes an experimental method of the sediment trapping and the results on the study of the variabilities of the flux of particulate matters at the different depths, regions and seasons.

2. Experimental

The sediment trap used here is made of polyvinyl chloride the size of which is 10.7 cm

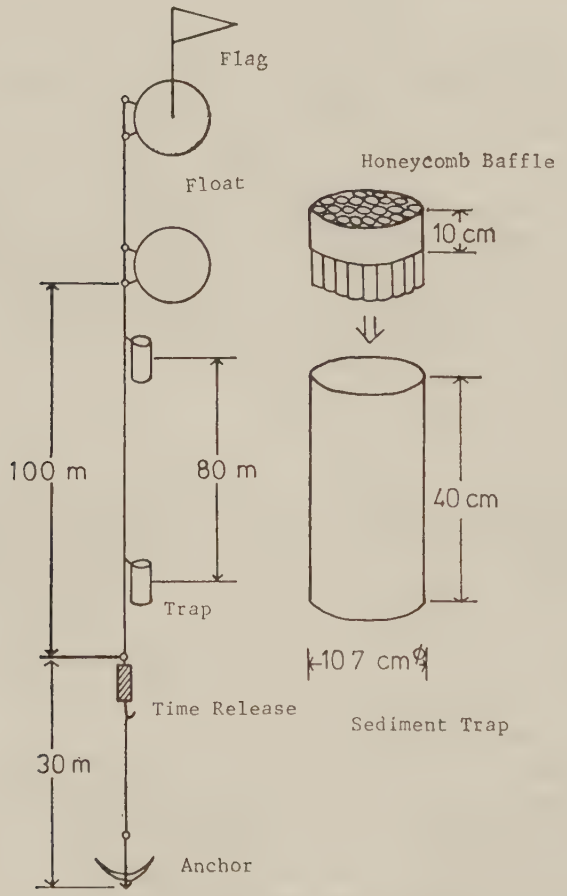

Fig. 1. The shape of the sediment trap and the sediment trap system which is consisted of two plastic floats, sediment traps, an electric time relaese and a 50 kg anchor all bound with 8 mm pylene eight rope.

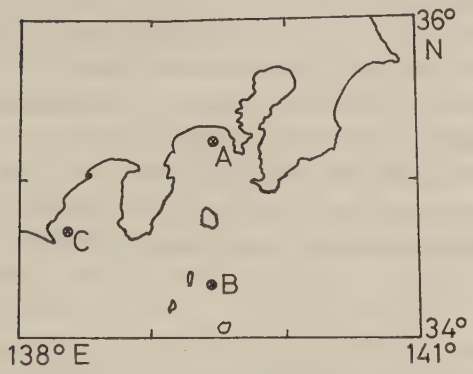

Fig. 2. Station location of the sediment trap systems. A is in Sagami Bay, B is near Niijima and C is in Suruga Bay.

diameter and 40 cm in height as shown in Fig. 1. To avoid the loss of the collected matter by the flowing out in the course of the retrieve of the system, the honeycomb baffle is attached to the upside of the sediment trap as recommended by G.A. KNAUER et al. (1979).

The system is consisted of two plastic floats, two or more sediment traps and an electric time release and an anchor which are all attached to 8 mm pylene eight rope as shown in Fig. 1. Plastic floats and electric time release are made for high water pressure registered.

After setting up the system on board the R.V. Ryofu-Maru, the floats are thrown first on the sea surface from the deck of the vessel, thereafter the traps and the time release are thrown successively. The anchor is thrown into the sea last, then the location and the water depth of the sediment trap system are determined by the long range navigation system of the type C (Loran C) and by the acoustic depth recorder, respectively. After about a week or more of the observation the vessel is moved to the accurate location by using the Loran C system at the expected releasing time. The sediment trap system is released from the anchor at the setting time by the electric time release. The yellow and the orange colored floats are looked for and found by human eyes on board the vessel. After approaching the vessel near the system, the free rope between the floats is picked up first and then all of the system without the anchor is retrieved.

The locations for the settling of the sediment trap systems are shown in Fig. 2. The systems were settled in Sagami Bay in October 1983 for 22 days, in March 1984 for 3 days, in May 1984 for 5 days and in October 1984 for 22 days (point A), and near Niijima (point B) for 22 days and Suruga Bay (point C) for 4 days in October 1984.

Particulate matters in sediment traps are collected on glass fiber filter (Whatmann GF/F). The filter on which the particulate matters are collected is boiled in a pressure resisting bottle with potassium peroxodisulfate solution. The oxidized solution is analyzed as phosphate-phosphorus by the automated system of the molibudenum blue colorimetric method. Another filter on which the particulate matters are also collected is extracted in acetone solution and two plant pigments, chlorophyll a and phaeophytin, are measured

by the fluorometric method successively. In this paper sum of two plant pigments is called total pigments. The principle of the analytical procedure is described in the manual reported by T.R. PARSONS, Y. MAITA and C.M. LALLI (1984).

At the same time of retrievement of the system, water samples are collected by Niskin bottles. Suspended matters are analyzed by the same method as the one for the sinking particles mentioned above and other typical components such as temperature, salinity, dissolved oxygen, phosphate and nitrate are also analyzed. Mean sinking velocity is given by the ratio of sinking fiux to suspended matter concentration at the same depth.

3. Results and remarks

Figire 3 shows vertical distribution of suspended matter and other analyzed components in Sagami Bay (Fig. 3-a, b, c, d) in three seasons except summer, near Niijima (Fig. 3-e) in October 1984 and in Suruga Bay (Fig. 3-f) in October 1984. In all observed seasons in Sagami Bay (Fig. 3-a, b, c, d) water temperature and dissolved oxygen decreases grad-

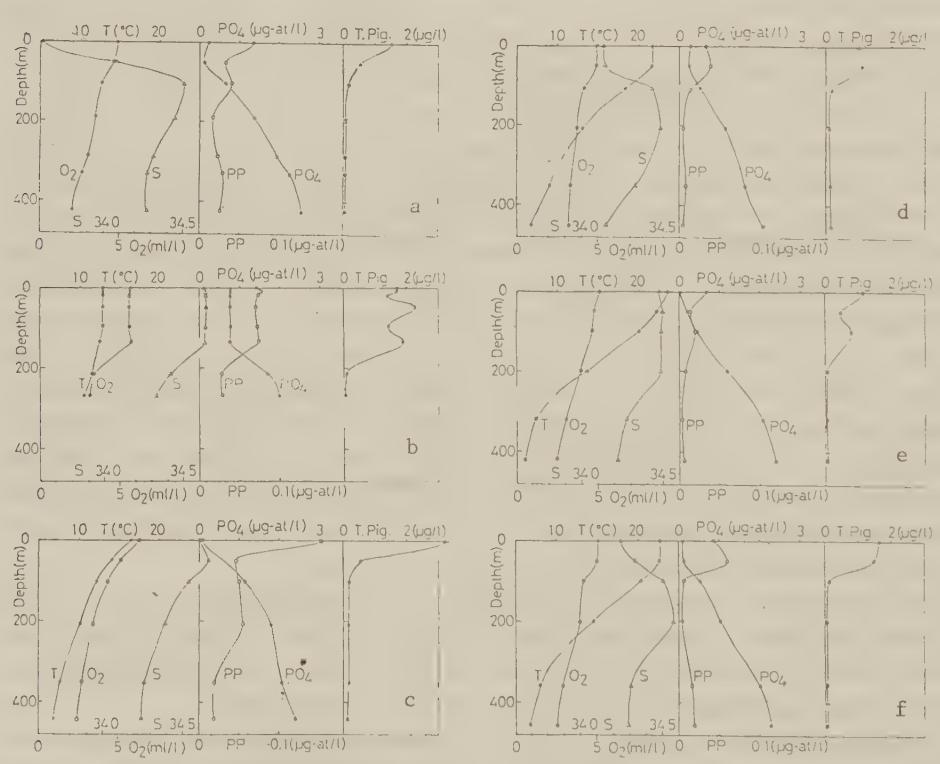

Fig. 3. Vertical distribution of water temperature, salinity, dissolved oxygen, phosphate, particulate phosphorus and total pigments at the same station as the systems. The observations of a), b), c) and d) were carried out in Oct. 1983, March 1984, May 1984 and Oct. 1984, respectively at the station A. The observations of e) and f) were carried out in the stations B and C, respectively in Oct. 1984.

ually with the increase of depth. Salinity shows low values at sea surface, especially in autumn, but it has the maximum values in the upper 200 m depths and decreases with the increase of depth. Particulate phosphorus and total pigments show large values in the upper layer and decrease with the increase of depth in all observed seasons, especially in spring these phenomena are clear. From the relatively large depth of the surface mixing layer shown in Fig. 3-b, it is suggested that the oceanographic condition in Sagami Bay in this season is still winter type even if it is March. In the comparison of Fig. 3-e (near Niijima) and Fig. 3-f (in Sagami Bay), the latter shows the clear maximum in salinity and this fact suggests the large influence of the coastal water in Suruga Bay. Particulate phosphorus and total pigments in the upper layer in Suruga Bay show larger values than that near Niijima.

Figure 4 shows the variation of flux and sinking velocity of the particulate matters with depths and regions in October 1984. The fluxes of phosphorus and total pigments vary nearly in parallel. This means that the origin of particulate phosphorus is living matters. The variations of the flux and of the sinking velocity with depth are not large in both phosphorus and total pigments. The ratio of the largest value to the smallest one does not exceed 3. The flux of the particulate matter in the upper layer is not always larger than that in the lower layer. The ratio of the largest value to smallest one in sinking velocities also does not exceed 3.

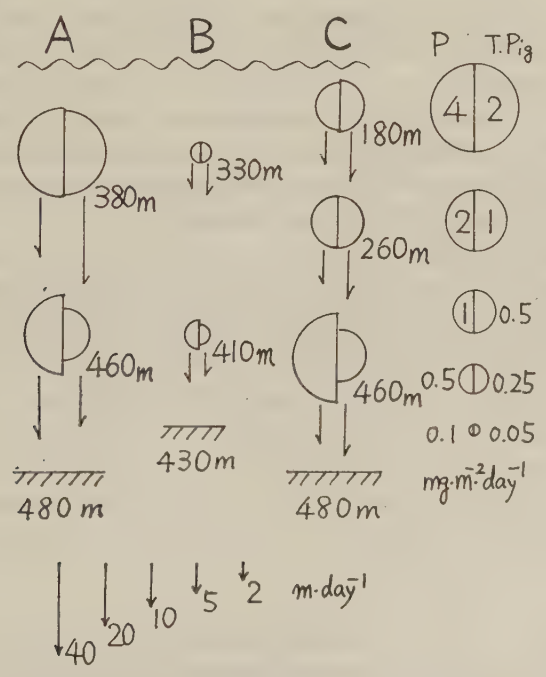

Fig. 4. Sinking flux (circle) and mean sinking velocity (arrow) of phosphorus (P) and total pigments (T. Pig.) at the stations, A, B, and C in October 1984.

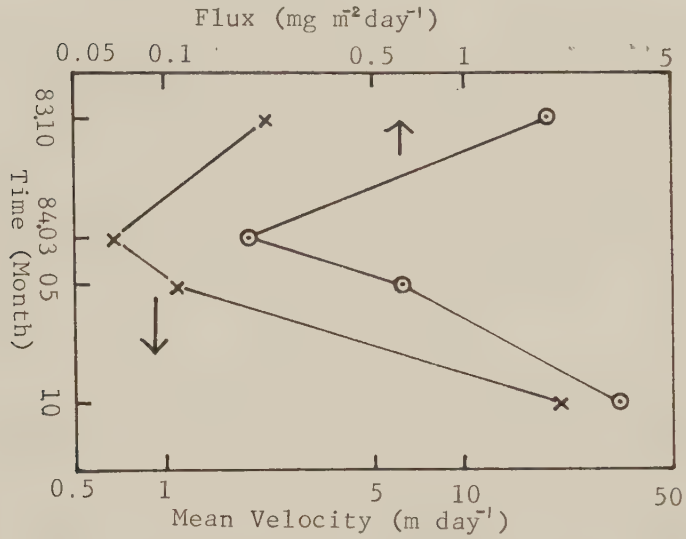

Fig. 5. Seasonal variation of the sinking flux (⊙) and the mean velocity (×) of phosphorus during Oct. 1983 to Oct. 1984 in Sagami Bay.

The regional variation of the flux is larger than that with depth as shown in Fig. 4. Fluxes of the particulate matters of A and C are in about the same order, but the flux at B in the off-shore area is 1 order lower than those at the coastal stations. The regional variation of the sinking velocity is also large but the ratio to each other is not larger than 1 order. This fact that the flux decreases with the distance from the land shows that the pollutant matters loaded to the sea water from the land area such as phosphorus sink rapidly and are eliminated from the sea water in the coastal region.

In addition to comment, the Kuroshio flew near off the point B during the observations.

The seasonal variations of phosphorus and plant pigments fluxes in the sinking particles at the point A (Sagami Bay) are shown in Fig. 5. The flux of the sinking particles observed at A decreases by 1 order from autumn (October) to winter (March) and increases in spring (May) and autumn (October) by the same order. The sinking velocity is small in winter and is large in autumn.

It is summarized that the flux of the sinking particles varies much both seasonally and regionally, but varies little with depth. The fact of the large regional variation of the flux shows that phosphorus loaded from the land area is removed before reaching the Kuroshio.

Acknowledgements

The author wishes to thank the observers, officers and crews of R/V Ryofu Maru for their co-operation on board. He also appreciates Mr. M. Iami for his analysis of plant pigments. This study is supported by the Self-Purification Project which Marine Depart-

ment of the Japan Meteorological Agency is charged with, in the Kuroshio Exploitation and Research Program (KER) promoted by the Science and Technology Agency of Japan.

References

FUJITA, N. and S. NISHIZAWA (1982): Vertical flux of particulate matter in the Antarctic Ocean in summer 1981. Trans. Tokyo Univ. Fisheries, **No. 5**, March, 43–52.

ISEKI, K. (1981): Vertical transport of particulate organic matter in the deep Bering Sea and Gulf of Alaska. J. Oceanogr. Soc. Japan. **37**, 101–110.

Japan Meteorological Agency (1985): Settling particles in the coastal region. KER Summary Report (1977–1982), 58.

KARL, D. M. and G. A. KNAUER (1984): Vertical distribution, transport and exchange of carbon in the northeast Pacific Ocean: Evidence for multiple zones of biological activity. Deep-Sea Res. **31**(3), 221–243.

KNAUER, G. A. and J. H. MARTIN (1981): Phosphorus-Cadmium cycling in northeast Pacific waters. J. Mar. Res., **39**(1), 65–76.

KNAUER, G. A., J. H. MARTIN and K. W. BRULAND (1979): Fluxes of particulate carbon, nitrogen and phosphorus in the upper water column of the northeast Pacific. Deep-Sea Res., **26A**, 97–108.

NORIKI, S., N. ISHIMORI, K. HARADA and S. TSUNOGAI (1985): Removal of trace metals from seawater during a phytoplankton bloom as studied with sediment traps in Funka Bay, Japan. Mar. Chem., **17**, 75–89.

PARSONS, T. R., Y. MAITA and C. M. LALLI (1984): A manual of chemical and biological method for sea water analysis. Pargamon Press, New York, U.S.A., pp. 173.

東京近海の沈降粒子

加納裕二
（気象庁）

陸水から負荷された様々な物質は黒潮へいたるまでに生化学的に変質し，海洋表層から除去されている可能性がある．このことを確かめるために，海中の沈降粒子を直接採集する装置（セディメントトラップ）を作製し，使用した．1983～1984年にかけて計4回東京近海（相模湾，駿河湾，新島付近）において観測船凌風丸によってセディメントトラップを設置し，沈降粒子を採集してその粒子中のリンや植物色素を測定した．相模湾での実験からリンの沈降量は秋に多く冬に少なく，また深度によってはあまり変化しないことがわかった．1984年10月の海域を変えての実験からは，リンや植物色素の沈降量は相模湾と駿河湾ではともに値が大きくその違いはわずかであるが，新島付近では相模湾や駿河湾に比して値が小さいことがわかった．これらの事実は陸水から負荷されたリンは黒潮へ拡散し混合する以前に生化学的に変質し，大部分が海洋表層から除去されていることを示している．この研究は黒潮開発利用調査研究（科学技術庁）の「黒潮浄化能力の把握プロジェクト」（気象庁担当）の一部としてなされた．

The Oceanographical Magazine
Vol. 36, Nos. 1-2, pp. 51 to 55, March 1986

NOTE

Long-term variations of sea surface temperature in the North Pacific Ocean

Masaro SAIKI and Koichi NAGASAKA
Japan Meteorological Agency

(Received December 26, 1985; Accepted January 20, 1986)

1. Introduction

Recently, there has been increasing interest in the fluctuations on climate in time scale of months, seasons, years and a few decades. In a number of intensive relevant studies thermal structure of the upper portions of the oceans, in particular anomalies of sea surface temperature, has been revealed to play one of the vital roles in those fluctuations of the atmosphere. Among major oceans the tropical Pacific has the most significant signals of a few years period in the variations of the sea surface temperature associated with the El Niño Events, that closely link to the climatic changes on the globe.

The current brief note is aimed to present some of statistical characteristics of the variation of monthly sea surface temperatere in the North Pacific Ocean including the tropical waters.

2. Data sources and data processing

Sea surface temperature data for the present investigation were prepared from the analysis charts operationally issued from both the Japan Meteorological Agency (JMA) and the National Oceanic and Atmospheric Administration of the US (NOAA). For the western North Pacific, ten-day mean charts from 1950 through 1985 in the JAM's Ten-Day Marine Reports were subjectively read out at each grid point in 1 degree in latitude

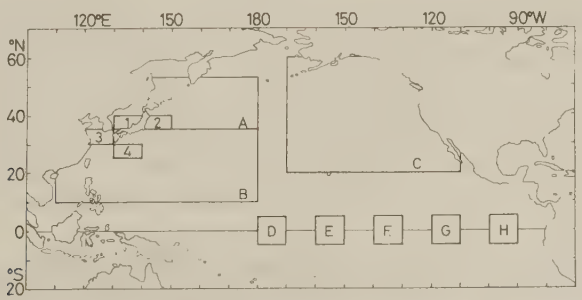

Fig. 1. Geograohical areas for the statistical investigation of sea surface temperature anomalies in the North Pacific Ocean.

by 1 degree in longitude meshes. Monthly tempertaures were obtained as arithmetic averages of ten-days' values in the relevant month. On the other hand, for the eastern North Pacific monthly charts in the NOAA's Fishing Information from 1947 through 1980 and Oceanographic Monthly Summary from 1981 through 1985 were digitized at each 5-degree by 5-degree grid point.

In this study the monthly anomalies of sea surface temperature, deviations from the climatological values for the 30-year from 1951 through 1980, were processed and time

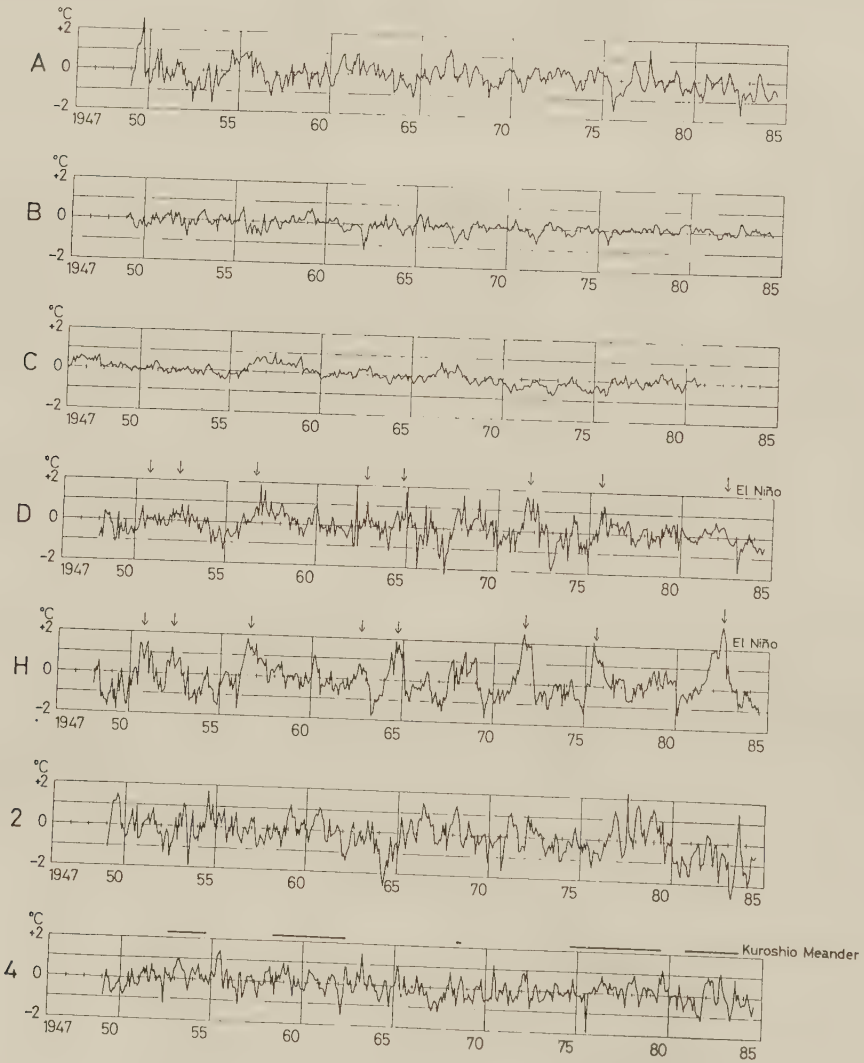

Fig. 2. Monthly mean anomalies of the sea surface temperatures in the regions given in Fig. 1. Arrows show the mature-phases of significant El Niño events and bars indicate periods in presence of large-meander in the path of the Kuroshio in south of Honshū.

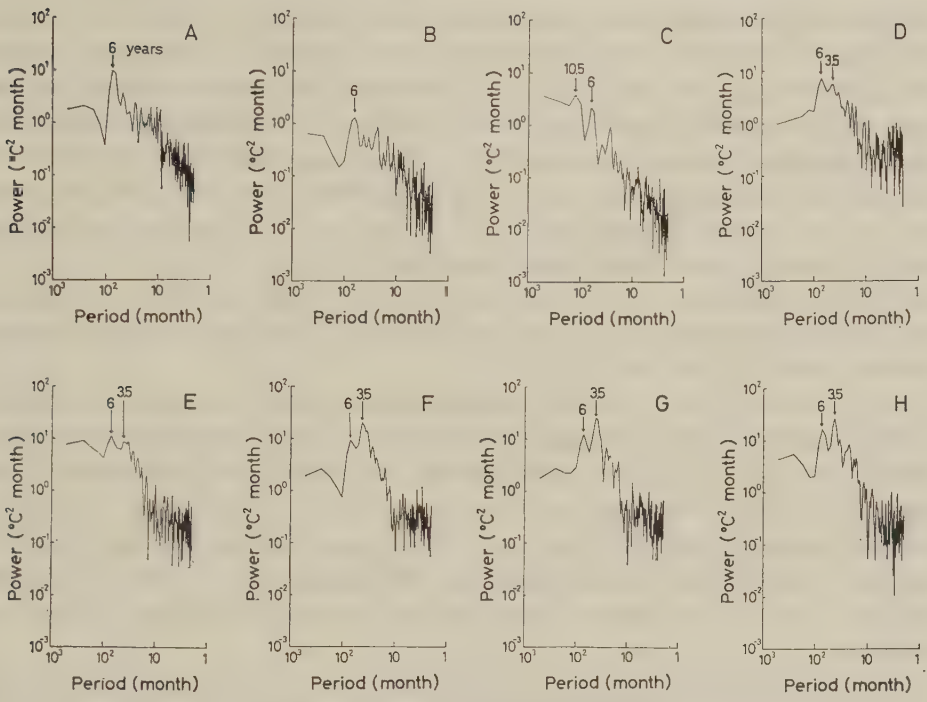

Fig. 3. Power spectra of the time-series illustrated in Fig. 2.

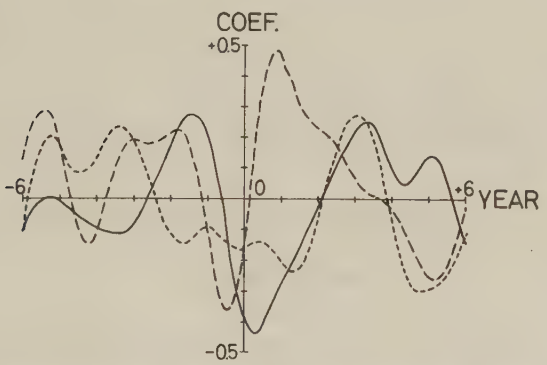

Fig. 4. Lagged correlation coefficients of the anomalies between the region H and the region A (solid line), between H and B (dashed line), and, between H and 2 (dotted line). +1 in the axis of years indicates that fluctuations in the region H are 1 year ahead of those concerned.

series of areal averages of those anomalies for the regions in Fig. 1 were reproduced in Fig. 2. Based on the time series analyses of spectra and various cross-correlations were carried out. Some of those results were illustrated in Fig. 3 and Fig. 4.

3. Brief description of statistical characteristics

Major features of the sea surface temperature fluctuations extracted by inspection of

those materials are briefly summarized as follows:

(1) 6-year is commonly recognized as one of dominant periods in the fluctuations not only in the mid-ocean (the regions from A through H) in the North Pacific Ocean but also in the waters adjacent to Japan (the regions 1 through 4). The 6-year fluctuations have been already found in the various oceanic phenomena in upper layers, for examples, in sea surface temperature in the North Pacific Ocean (Favorite *et al.*, 1973, and Teramoto, 1974) and the Tsushima Straights (Mita *et al.*, 1984) as well as in the geostrophic volume transport of the Kuroshio in the Eastern China Sea (Saiki, 1982).

(2) The fluctuations in the Japan Sea (the region 1) is highly correlated with those of 1 month to 2 months before in the Eastern China Sea (the region 3). The correlation coefficient between the two reaches +0.75.

(3) In the western North Pacific, the fluctuations are out of phase between the northern area (the region A) and the southern area (the region B). One of peaks in the lagged correlation coefficient, −0.48, is recognized between the fluctuations in the southern area and those of 1 year before in the northern area.

(4) In the eastern North Pacific (the region C) 10.5-year fluctuations are slightly notable as well as those in 6-year. In the years from 1969 through 1976 the temperature were continuously below the climatological level and the mean of the deviations for the period reaches to −0.3°C.

(5) In the eastern tropics 3.5-year fluctuations are more dominant in comparison with those in 6-year, and this period corresponds to the mean of the intervals between two suc-

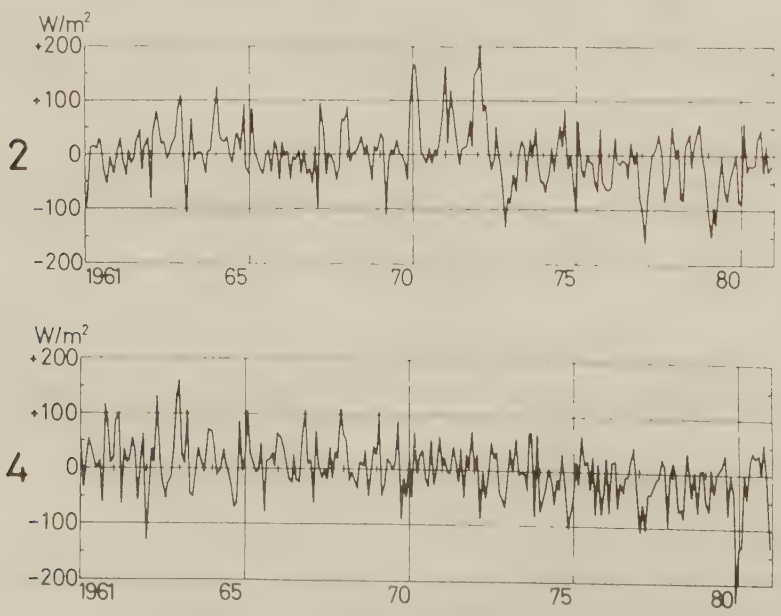

Fig. 5. Monthly anomalies of heat flux obtained by the bulk method through the sea surface in the regions 2 and 4. Positive in vertical axis means that the ocean gains more heat compaired with the long-term average.

cessive El Niño Events. The easter the region is located, the larger the ratio of the amplitude of 3.5-year fluctuations to those of 6-year becomes.

(6) The correlation coefficent has a negative peak value, −0.44, between the fluctuations in the eastern tropics (the region H) and those of 3 months after in the northern portion of the western North Pacific (the region A). Namely, the sea surface temperature in the region A has a tendency in negatively deviating from the climatological level during El Niño Events.

The fluctuation in the southern portion of the western North Pacific (the region B) are correlated positively (the correlation coefficient; +0.48) with those of 1 year before and negatively (−0.36) with those of 6 months after in the eastern tropics (the region H), respectively.

Figure 5 shows the fluctuations of the anomalies of the heat flux through the sea surface in the waters adjacent to Japan, the regions 2 and 4, obtained by using a bulk method based on the marine meteorological data set prepared by the JMA. From these figures some of general trends are clearly identified. However, no simple correlations were observed between the time series of sea surface temperatures and heat exchanges in the individual waters. Further comprehensive studies on the mutual interaction between the ocean and atmosphere on a global basis as well as on a local basis are required.

References

FAVORITE, F. and D. R. MCLAIN (1973): Coherence in transpacific movements of positive and negative anomalies of sea surface temperature. Nature, **244**, 139–143.

MIITA, T. and S. TAWARA (1984): Seasonal and secular variations of sea water temperature in the East Tsushima Strait. J. Oceanogr. Soc. Japan, **40**, 91–97.

SAIKI, M. (1982): Relation between the geostrophic flux of the Kuroshio in the Eastern China Sea and its large-meander in south of Japan. Oceanogr. Mag., **32**, 11–18.

TERAMOTO, T. (1974): Aims of programme for investigations on the air-sea interaction in the North Pacific Ocean (NORPAX). (in Japanese) Kagaku, **44**, 685–693.

北太平洋の海面水温の長期変動について

佐伯理郎・長坂昂一
（気象庁）

赤道域を含む北太平洋の月平均海面水温偏差の時系列データ（1947～85年）をもとに，スペクトル解析などによって，その長期変動について調べた．その結果，北太平洋全域で6年周期の変動が卓越していること，エル・ニーニョ発生海域である東部太平洋赤道域ではその発生平均間隔である3.5年周期の変動も大きく，この海域と北西太平洋の間には1年以内のズレで比較的高い相関関係がみられることなどがわかった．

The Oceanographical Magazine
Vol. 36, Nos. 1–2, pp. 57 to 62, March 1986

NOTE

Cadmium and mercury in the seas around Japan

Takeshi SAGI
Japan Meteorological Agency

(Received November 11, 1985; Accepted January 14, 1986)

1. Introduction

The surveys of the background level of heavy metals concentration in sea water are very important in relation to the marine environmental pollution. Determinations of two heavy metals (cadmium and mercury) have been made in each season since 1972 on lines across the Kuroshio or the Kuroshio Extension in the seas around Japan. Based on these data, SAGI et al. (1974) gave the average values of cadmium for the surface (60 ng/kg) and the deep water (110 ng/kg) in the western North Pacific, and SUZUOKI (1983) reported the time and spacial distribution (1972–1981) of cadmium in marine environment around Japan.

The report presented here describes the background levels of cadmium and mercury concentration in sea water and the year to year changes of cadmium concentration in the seas around Japan, based on the monitoring data reported by the Japan Meteorological Agency (1973–1985).

2. Sampling and analytical method

Sea water samples are collected by using Niskin bottles and stored in polyethylene bottles

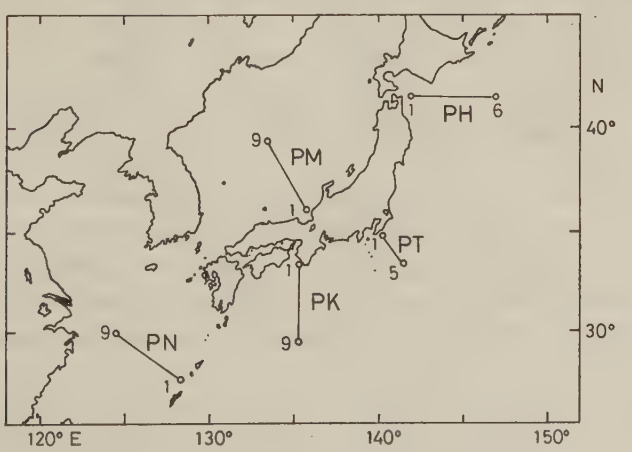

Fig. 1. Observation lines and sampling stations.

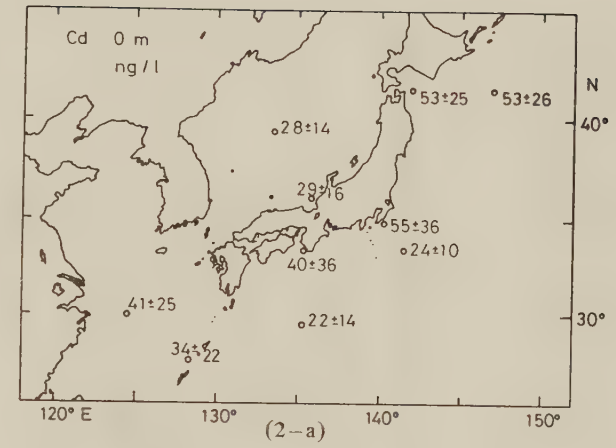

(2−a)

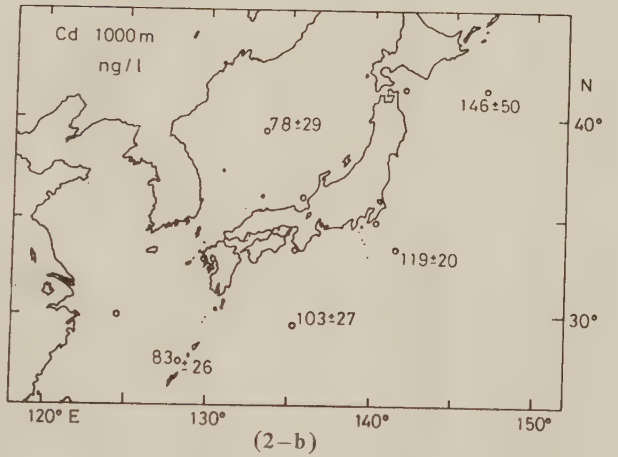

(2−b)

Fig. 2. Mean concentrations during 1982–1984 of cadmium in the surface water (2-a) and in the deep water (2-b).

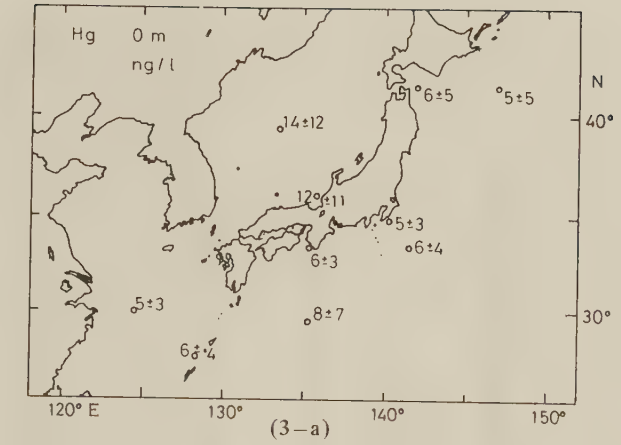

(3−a)

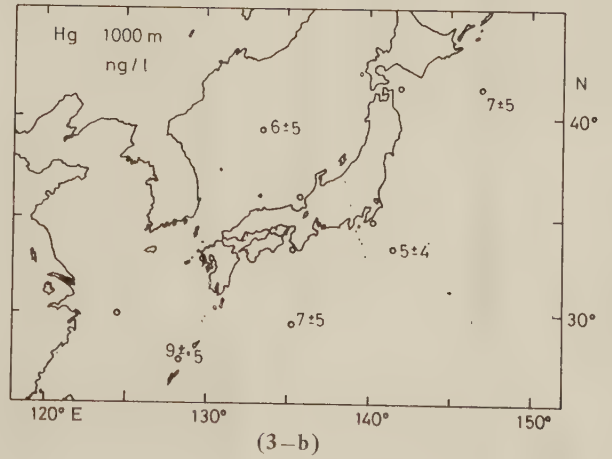

(3−b)

Fig. 3. Mean concentrations during 1982–1984 of mercury in the surface water (3-a) and in the deep water (3-b).

for cadmium and in glass bottles for mercury after adding HCl and H_2SO_4, respectively.

Cadmium in 75 ml of sea water sample is extracted into APDC-DDTC-chloroform, followed by the back extraction using 3 ml of 1 N HCl solution and analyzed by the atomic absorption spectrophotometry coupled with graphite atomizer.

Mercury in 250 ml of sea water sample is analyzed by the flameless atomic absorption spectrophotometry using the $SnCl_2$ reduction method. For the sake of prevention from the environmental contamination, the atmosphere in the system is kept clean with the air passed through the column filled up by particles of gold.

The detection limits in these methods are as low as 5 ng/kg (Cd) and 1 ng/kg (Hg), and the analytical errors are estimated to be within ± 5 ng/kg (Cd) and ± 1 ng/kg (Hg) at the concentration levels of the sea water, respectively.

Observation lines and sampling stations are shown in Fig. 1, where the samples are taken in each of season.

3. General features in the distribution of cadmium

The average concentrations and their standard deviations of cadmium in sea water in the last three years (1982–1984) in the seas around Japan are shown in Fig. 2. In the surface water (Fig. 2-a), the concentrations are high (50 ng/kg) in the regions off Boso peninsula (PT 1) and south of Hokkaido (PH 1, 6), rather high (40 ng/kg) on the continental shelf of the East China Sea (PN 9) and off the Kii Channel (PK 1), rather low (30 ng/kg) in the Japan Sea (PM 1, 9), and low (20 ng/kg) in the offshore regions south of Japan.

In the deep water (Fig. 2-b, at the depth of about 1000 m), relatively higher values (150 ng/kg) are found in the regions off the south of Hokkaido, while the lower values (80 ng/kg) are found in the Japan Sea. The values of about 100 ng/kg in the offshore regions south of Japan are lower than those in the regions off the south of Hokkaido but higher than those in the Japan Sea. Similar distributions have been found on the concentration of nutrients such as phosphorus and nitrate in sea water around Japan. It has been reported that the distributions of cadmium in the open ocean are strongly correlated with those of nutrients (for example, MATSUNAGA and ABE, 1985). It may be concluded that a background level of cadmium concentration is higher in the regions south of Hokkaido and is lower in the Japan Sea than those in other regions.

4. General features in the distribution of mercury

The average concentrations and their standard deviations of mercury in sea water in the last three years (1982–1984) in the seas around Japan are shown in Fig. 3. Although the mean values in the surface water fluctuate slightly with locations (Fig. 3-a), a background level of mercury concentration in sea water except for the Japan Sea is estimated to be about 6 ng/kg irrespective of the shore or the offshore region. Mercury concentration in the Japan Sea is significantly higher (10–15 ng/kg) than those in other regions. Since the values fluctuate so much (± 12 ng/kg), the factor affecting this high value is not clear.

In the deep water (Fig. 3-b, at the depth of about 1000 m), the concentrations are 6–7 ng/kg in the seas around Japan.

5. Year to year change of cadmium concentration

Year to year change of cadmium concentration in the seas around Japan is shown in Fig. 4 by three years moving average. Since 1979, the concentrations in the coastal regions

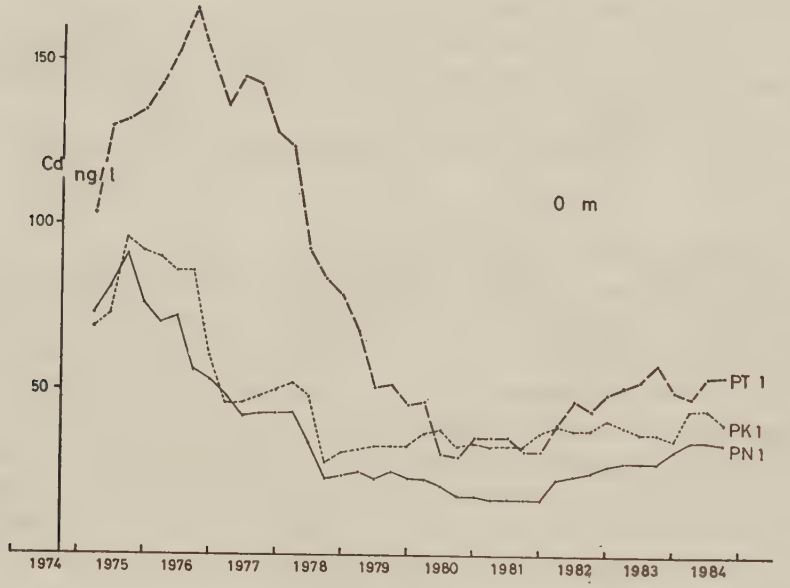

(4–a)

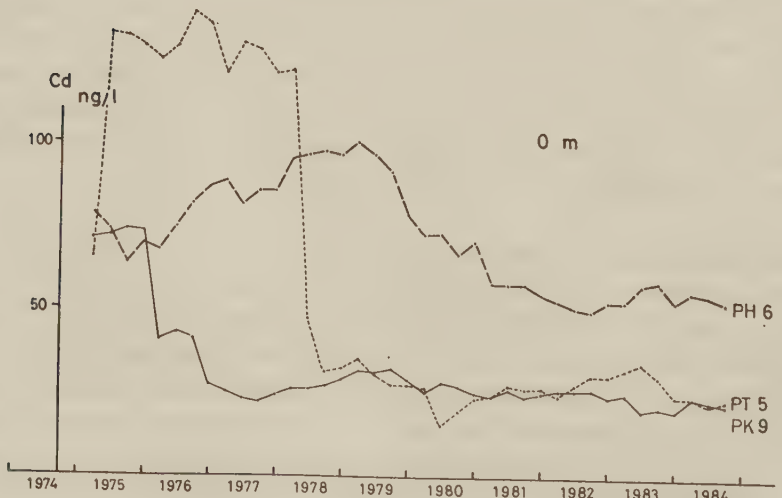

(4–b)

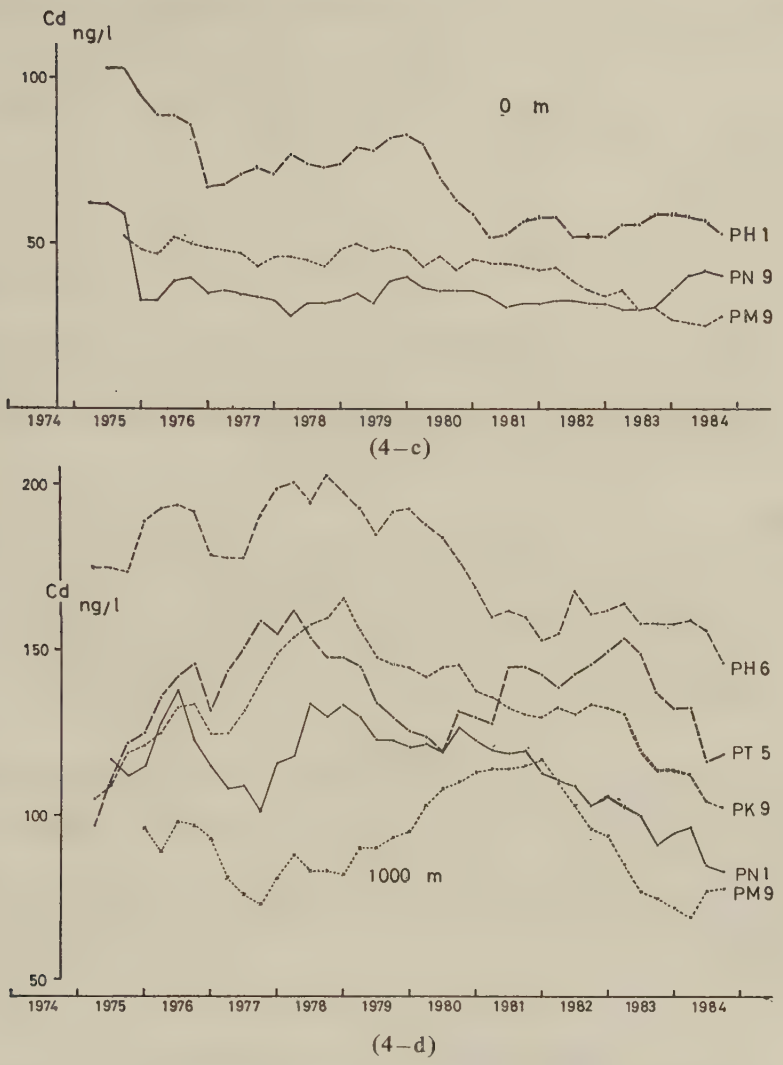

Fig. 4. Year to year change of cadmium concentrations in the coastal region (4-a), in the offshore region (4-b), off the Tsugaru Channel, in the East China Sea and in the Japan Sea (4-c), and in the deep waters (4-d).

(Fig. 4-a) are in nearly the same value in each region but increase toward the downstream of the Kuroshio in order of the regions along Ryukyu island (PN 1), off Kii Channel (PK 1) and off Boso Peninsula (PT 1). The concentrations in the offshore regions (Fig. 4-b) are in the low value (20–30 ng/kg) in the regions south of Japan (PT 5 and PK 9), and are in the high value (50–60 ng/kg) in the region south of Hokkaido. In the East China Sea (PN 9) and the Japan Sea (PM 9) (Fig. 4-c), the concentration are in the value of 30–50 ng/kg since 1976.

Table 1. The background levels of cadmium and mercury concentration in the seas around Japan.

	Cadmium		Mercury	
Sea area	0 m	1000 m	0 m	10000 m
South of Japan	40–50		5–6	
South of Hokkaido	50	150	5–6	7
East China Sea	40		5–6	
Japan Sea	30	80	12–14	6
Kuroshio region	20	100	6–8	6

unit: ng/kg

The concentrations in the deep waters (Fig. 4-d, at the depth of about 1000 m) are lower in the Japan Sea (PM 9) and higher in the region south of Hokkaido (PH 6) compared with other regions. It seems that the concentrations of cadmium show an annual trend of gradual decrease in any region around Japan since 1981.

6. Summary

Based on the data of cadmium (1981–1984) and mercury (1982–1984), the background level in the seas around Japan is summarized as shown in Table 1. Since 1981 in the seas around Japan, cadmium concentrations are in the same level in the surface waters and show a trend of gradual decrease in the deep waters. Due to the large fluctuation of the concentrations, an annual change of the mercury concentration is still uncertain.

References

Japan Meteorological Agency (1973–1985): Prompt Report of Observation for Monitoring Background Marine Pollution. Nos. **4–27**.

Matsunaga, M. and K. Abe (1985): Relationship between cadmium and phosphate in the north west Pacific Ocean. J. Oceanogr. Soc. Japan, **41**, 193–197.

Sagi, T., T. Yura and T. Akiyama (1974): The cadmium content in sea water in the adjacent regions of Japan and in the western North Pacific. Oceanogr. Mag., **25**, 101–110.

Suzuoki, T. (1983): Cadmium in marine environment around Japan during 1972–1981. Oceanogr. Mag., **33**, 51–54.

日本周辺海域のカドミウム及び水銀

鷺　猛

（気象庁　海洋気象部）

日本周辺海域について，カドミウムと水銀濃度のバックグラウンドレベルを求めた．カドミウムは海面では，黒潮域が最も低く (20 ng/kg)，親潮域と日本の南岸が高い (50 ng/kg)，日本海はこの中間 (30 ng/kg) にある．深層では親潮域が 150 ng/kg，日本海が 80 ng/kg で，黒潮域がその中間 (100 ng/kg) にある．

水銀は日本海の海面で若干高い (12～14 ng/kg) 外は海域による差は認められず，5～8 ng/kg の範囲にある．

経年的には，カドミウムは1981年以降，海面では横ばい状態にあるが，深層では漸減傾向にある．

昭和61年3月31日　発行

編集兼
発行者　気象庁
東京都千代田区大手町1の3の4

印刷者　青木俊夫

印刷所　昌美印刷株式会社
東京都千代田区飯田橋2の6の1